university of groningen

University of Groningen

Faculty of mathematics and natural sciences

Department of physics

Master Thesis

Strongly correlated electrons on a honeycomb lattice

Author:
C.P. van der Vegte
S1655426
Internal number: 373

Supervisors:
Prof. Dr. M. Mostovoy
Prof. Dr. T. Ogawa
Prof. Dr. A. Asano
Prof. Dr. A. Ohashi

Contents

Chapter 1

Introduction

Strongly correlated electron systems have fascinated physicists for decades. It started by the study of the metal-insulator transition also known as the Mott transition (Nobel prize 1977) which was observed in transition metal oxides, like for instance V_2O_3 in the late 1960's. This transition occurs when it is energetically favorable for the system to localize electrons when the Coulomb interaction between them becomes large compared to their kinetic energy. The study of strongly correlated electron systems continued and celebrated successes with the discovery of high T_c superconductivity in 1986 (Nobel prize 1987). The high T_c superconducting state, in which the material has zero resistance, is observed in certain Mott insulators upon doping by charge carriers and the mechanism still needs to be revealed.

Recently the field of strongly correlated electron systems was boosted by the discovery of graphene (Nobel prize 2010), a two dimensional material with a honeycomb lattice of carbon atoms. The electrons in graphene have a linear dispersion and thus are relativistic. This allows one to study some relativistic effects in a table-top experiment without needing a particle accelerator. Graphene has a high conductivity and, therefore, might be used in next-generation microelectronic devices. Graphene based transistors are expected to be much faster then the transistors used today made of Silicon. Graphene is a so-called semimetal and is conducting at room temperature.

In this report we study the Hubbard model on a two-dimensional honeycomb lattice with one electron per site (half filling). The Hubbard model [38] includes nearest neighbor hopping of electrons with amplitude t and on-site Coulomb interaction between electrons with strength U. We study the semimetal-insulator transition that is expected to occur for the honeycomb lattice when the ratio U/t is increased, similar to the Mott transition observed in transition metal oxides. This work is devoted to finding the critical value U_c/t for this transition, which has not jet been observed in graphene, to occur.

It is difficult to describe strongly correlated electron systems. First of all one has to deal with a large number of particles (ions,electrons). The Coulomb interaction between the electrons is of the same order as their kinetic energy and, therefore, perturbation theory does not apply. Even simple models describing electron correlations, like the Hubbard model, are extremely difficult to solve. An exact solution for the Hubbard model in the case of a one-dimensional chain exists, called the Bethe Ansatz [1]. For higher dimensions, however, an exact solution is not available and one has to rely on approximations. Mean field theories like the Hartree-Fock approximation for the Hubbard model are commonly used when dealing with many body systems. Such mean field theories substitute the interaction of an electron with other electrons by an interaction with a mean field. The Hartree-Fock approximation assumes that the probability for the occupation of a site by a spin-up electron is independent of the occupation of that site by a spin-down electron. When the Coulomb interaction between electrons is large, the double occupation of a site becomes energetically unfavorable and this approximation becomes invalid. Therefore, static mean field theories cannot describe strongly correlated electron systems. In this report we study the two-dimensional honeycomb lattice using two numerical techniques, called Dynamical Mean Field Theory and Cluster Perturbation Theory, that have been successfully applied to strongly correlated electron systems.

Dynamical Mean Field Theory (DMFT) gives an exact solution for the Hubbard model in the limit of infinite lattice coordination ($z \to \infty$). For a face-centered cubic lattice $z = 12 >> 1$, and so in real materials this limit can be achieved. In the limit of infinite lattice coordination the Hubbard model reduces to a single impurity site embedded in an effective medium. This is very similar to the Weiss mean field theory used in statistical mechanics for the Ising model. The effective medium in the case of DMFT is, however, not described by a static mean field, but it can exchange electrons with the impurity site. The theory is very powerful because it does not require the interaction to be small, and has been successfully used to describe the Mott transition [8].

DMFT studies a single site and, therefore, can only describe local electron correlations at the impurity site. Non-local electrons correlations (between electrons at neighboring sites)can be incorporated in cluster DMFT, which are computationally demanding. A different technique that includes non-local electron correlations is Cluster Perturbation Theory. In this theory the lattice is divided into identical small sized clusters (e.g. 16 sites maximum). Exact diagonalization is used to solve the Hubbard model on a single cluster, and the exchange of electrons between clusters is treated perturbatively.

This report proceeds as follows. In Chap. 2 the Hubbard model is derived and the nature of the Mott transition is explained. The limitations of static mean field theories, like the Hartree approximation, will be discussed.

Chap. 3 is dedicated to the formalism of single-site Dynamical Mean Field Theory. The chapters starts with a discussion on the Hubbard model in the limit of infinite lattice coordination. The equations describing the single impurity site in the effective medium will be derived and a numerical method for solving the equations is discussed. The theory will be applied to describe the metal-insulator transition for a Bethe lattice by calculating the density of states for different values of the ratio U/t.

In Chap. 4 we study the Hubbard model on a honeycomb lattice. First basic properties of the lattice, like the Brillouin zone and the band structure in the case of non-interacting electrons is calculated. Then we use single-site DMFT to study the semimetal-insulator transition for the honeycomb lattice.

In Chap. 5 Cluster Perturbation Theory will be used to include non-local electron correlations. The chapter starts by explaining the method and gives a detailed explanation of the numerical techniques used. The density of states and spectral weight for the honeycomb lattice for different values of U/t is calculated. From these results a critical value U_c/t, for the semimetal-insulator transition is predicted.

Chapter 2

Hubbard model

The Hubbard model named after John Hubbard is a simple model describing interacting electrons on a lattice. The model is commonly used in condensed matter physics to describe the metal-insulator (Mott) transition observed in various transition metal oxides. Transition metals have partially filled d shells that form narrow energy bands, which have great influence on the properties of the material. The average time spend by an electron on an atomic orbital is proportional to the inverse bandwidth ($\propto W^{-1}$). So the smaller the bandwidth, the longer an electron stays at an ion and the more it feels the presence of other electrons at that ion. Therefore, electron correlations are important in materials with narrow band, like transition metal oxides. The Coulomb interaction between electrons gives rise to the metal-insulator transition.

This chapter starts by a derivation of the Hubbard model. To get a better understanding of the model, a one dimensional chain will be studied using the Hartree approximation. Experimental results on the Mott transition for the transition metal V_2O_3 will be shown and discussed.

2.1 Hubbard model

The derivation of the Hubbard model can be found in many textbooks. Here we follow the derivation given in Ref. [1].

It is quite difficult to describe solids since there are many particles (electrons,ions) to consider. We are interested in the electronic properties of the solid. The ions form a periodic lattice structure and their positions are assumed to be fixed. The reasoning behind this approximation is that the masses of the ions are much larger then the electron masses and, therefore, their kinetic energy is small compared to that of the electrons. The Hamiltonian for N electrons in a solid can

be written as

$$\mathcal{H} = \sum_{i=1}^{N} \frac{\mathbf{p}_i^2}{2m} + \sum_{i=1}^{N} V_I(\mathbf{x}_i) + \frac{1}{2}\sum_{i\neq j} V_c(\mathbf{x}_i - \mathbf{x}_j), \tag{2.1}$$

where the first term is the kinetic energy of the electrons, the second term is the interaction of the electrons with the external potential created by the ions and the third term denotes the Coulomb interaction between electrons

$$V_c(\mathbf{x}_i - \mathbf{x}_j) = \frac{e^2}{|\mathbf{x}_i - \mathbf{x}_j|}. \tag{2.2}$$

It is very difficult to solve this Hamiltonian exactly because of the large number of particles and the two-particle potential $V_c(\mathbf{x}_i - \mathbf{x}_j)$. Mean field theories commonly used to solve such many body Hamiltonians, are based on adding a potential $V_A(\mathbf{x})$ to the one-particle part of the Hamiltonian and subtracting it from the two-body coulomb part

$$\begin{aligned} V(\mathbf{x}_i) &= V_I(\mathbf{x}_i) + V_A(\mathbf{x}_i) \\ U(\mathbf{x}_i, \mathbf{x}_j) &= V_c(\mathbf{x}_i - \mathbf{x}_j) - \frac{1}{N-1}(V_A(\mathbf{x}_i) + V_A(\mathbf{x}_j)). \end{aligned} \tag{2.3}$$

The Hamiltonian in Eq. (2.1) can then be rewritten as

$$\mathcal{H} = \sum_{i=1}^{N} \frac{\mathbf{p}_i^2}{2m} + \sum_{i=1}^{N} V(\mathbf{x}_i) + \frac{1}{2}\sum_{i\neq j} U(\mathbf{x}_i, \mathbf{x}_j). \tag{2.4}$$

In a mean field theory the potential $V_A(\mathbf{x})$ is chosen such that the two body part of the Hamiltonian $U(\mathbf{x}_i - \mathbf{x}_j)$ is small compared to the single body part. The potential $V_A(\mathbf{x})$ is then chosen as the average repulsive potential at the point $\mathbf{x}$, created by all electrons.

The potential $V(\mathbf{x}_i)$ is a periodic function with the periodicity of the lattice, since the positions of the ions are fixed. The eigenfunctions of the single-body part of the Hamiltonian are Bloch functions,

$$\left(\sum_{i=1}^{N} \frac{\mathbf{p}_i^2}{2m} + \sum_{i=1}^{N} V(\mathbf{x}_i)\right) \psi_{\alpha\mathbf{k}}(\mathbf{x}) = \epsilon_{\alpha\mathbf{k}} \psi_{\alpha\mathbf{k}}(\mathbf{x}), \tag{2.5}$$

where

$$\psi_{\alpha\mathbf{k}}(\mathbf{x}) = u_{\alpha\mathbf{k}}(\mathbf{x}) e^{i\mathbf{k}\cdot\mathbf{x}}. \tag{2.6}$$

Here α is an index denoting the band and $\mathbf{k}$ is the momentum. Note that the function $u_{\alpha\mathbf{k}(\mathbf{x})}$ has the periodicity of the lattice. It is convenient to define a basis using Wannier functions, $\phi_\alpha(\mathbf{x}-\mathbf{R}_i)$, centered around the lattice site with lattice vector R_i

$$\phi_\alpha(\mathbf{x} - \mathbf{R}_i) = \frac{1}{\sqrt{L}} \sum_{\mathbf{k}} e^{-i\mathbf{k}\cdot\mathbf{R}_i} \psi_{\alpha\mathbf{k}}(\mathbf{x}). \tag{2.7}$$

The Wannier functions are orthogonal for different band (α) and site (i) indices. The Bloch function is related to the Wannier function via the inverse Fourier transform

$$\psi_{\alpha\mathbf{k}}(\mathbf{x}) = \frac{1}{\sqrt{L}} \sum_{\mathbf{k}} e^{i\mathbf{k}\cdot\mathbf{R}_i} \phi_\alpha(\mathbf{x} - \mathbf{R}_i), \tag{2.8}$$

The creation operator of an electron with spin projection σ, in the Bloch state $\psi_{\alpha\mathbf{k}}$ is defined as $c^\dagger_{\alpha\mathbf{k}\sigma}$. The field operator creating an electron at position $\mathbf{x}$ with spin σ is then given by

$$\Psi^\dagger_\sigma(\mathbf{x}) = \sum_{\alpha\mathbf{k}} \psi^*_{\alpha\mathbf{k}}(\mathbf{x}) c^\dagger_{\alpha\mathbf{k}\sigma} = \sum_{\alpha i} \phi^*_\alpha(\mathbf{x} - \mathbf{R}_i) c^\dagger_{\alpha i\sigma}. \tag{2.9}$$

In terms of this field operator the Hamiltonian in Eq. 2.1 can be written as

$$\begin{aligned} \mathcal{H} &= \sum_\sigma \int dx^3 \Psi^\dagger_\sigma(\mathbf{x}) \left(\frac{\mathbf{p}^2}{2m} + V(\mathbf{x}) \right) \Psi_\sigma(\mathbf{x}) \\ &+ \frac{1}{2} \sum_{\sigma\sigma'} \int dx^3 \int dy^3 \Psi^\dagger_\sigma(\mathbf{x}) \Psi^\dagger_{\sigma'}(\mathbf{y}) U(\mathbf{x},\mathbf{y}) \Psi_{\sigma'}(\mathbf{y}) \Psi_\sigma(\mathbf{x}) \end{aligned} \tag{2.10}$$

Using second quantization (Eq. 2.9) the Hamiltonian in the basis of the Wannier states is given by

$$\mathcal{H} = \sum_{ij\alpha\sigma} t^\alpha_{ij} c^\dagger_{\alpha i\sigma} c_{\alpha i\sigma} + \frac{1}{2} \sum_{\alpha\beta\gamma\delta} \sum_{ijlm} \sum_{\sigma\sigma'} U^{\alpha\beta\gamma\delta}_{ijlm} c^\dagger_{\alpha i\sigma} c^\dagger_{\beta j\sigma} c_{\gamma l\sigma'} c_{\delta m\sigma}, \tag{2.11}$$

where,

$$\begin{aligned} t^\alpha_{ij} &= \int dx^3 \phi^*_\alpha(\mathbf{x} - \mathbf{R}_j) \left(\frac{\mathbf{p}^2}{2m} + V(\mathbf{x}) \right) \phi_\alpha(\mathbf{x} - \mathbf{R}_j) \\ &= \frac{1}{L} \sum_{\mathbf{k}} e^{i\mathbf{k}\cdot(\mathbf{R}_i - \mathbf{R}_j)} \epsilon_{\alpha\mathbf{k}} \end{aligned} \tag{2.12}$$

$$U^{\alpha\beta\gamma\delta}_{ijml} = \int dx^3 dy^3 \phi^*_\alpha(\mathbf{x} - \mathbf{R}_i) \phi^*_\beta(\mathbf{y} - \mathbf{R}_j) U(\mathbf{x},\mathbf{y}) \phi_\gamma(\mathbf{y} - \mathbf{R}_m) \phi_\delta(\mathbf{x} - \mathbf{R}_l). \tag{2.13}$$

The hopping matrix t^α_{ij} describes the possibility for an electron in the band α to hop from the site i to the site j. In band theory the electron correlation term (Eq. 2.13) is often neglected or treated perturbatively under the assumption that the hopping matrix elements are much larger ($t^\alpha_{ij} >> U^{\alpha\beta\gamma\delta}_{ijml}$).

In the Hubbard model the Coulomb interaction parameters are taken into account. It is assumed however, that the Coulomb interaction between two electrons located at different ions is negligible, compared to the Coulomb interaction

between two electrons located at the same site. The only nonzero components of the Coulomb interaction matrix are then the diagonal elements in site indices $U_{iiii}^{\alpha\beta\gamma\delta}$.
The band indices can be dropped if only a single band is important. This is the case when the whole Fermi surface lies in a single band and the other bands have much higher energies, so that the interactions between bands are weak. Under these assumptions the Hamiltonian in Eq. 2.11 reduces to

$$\mathcal{H} = \sum_{ij} t_{ij} c_{i\sigma}^{\dagger} c_{j\sigma} + \frac{U}{2} \sum_{i} c_{i\sigma}^{\dagger} c_{i\sigma'}^{\dagger} c_{i\sigma'} c_{i\sigma}. \tag{2.14}$$

The first term describes the hopping of electrons between different ions. If only the nearest neighbor hopping with the amplitude t is considered, the Hubbard Hamiltonian reduces to

$$\mathcal{H}_H = -t \sum_{<ij>,\sigma} c_{i\sigma}^{\dagger} c_{j\sigma} + U \sum_{i} n_{i\uparrow} n_{i\downarrow}, \tag{2.15}$$

where $n_{i\sigma}$ is the occupation number of an electron, with spin projection σ, at the site i,

$$n_{i\sigma} = c_{i\sigma}^{\dagger} c_{i\sigma}. \tag{2.16}$$

The first term in Eq. (2.15) corresponds to the tight-binding model where the electrons are tightly bound to their atoms. The wave functions of the electrons are almost the same as the wave functions of the atomic orbitals. When atoms are located close to each other, the tight-binding model allows an electron to sometimes leave it's atomic orbital and jump to a neighboring atom. Narrow bands are formed because the orbitals of neighboring atoms overlap. The second term in Eq. 2.15 describes the Coulomb interaction between two electrons that are located at the same atom. The degeneracy of the atomic orbital is neglected so that the maximum number of electrons at a single site is two, due to the Pauli principle.

2.2 Metal-insulator transition for a one-dimensional chain

In this section a one-dimensional chain of N atoms and lattice constant a with periodic boundary conditions is considered. Using the Hartree approximation it will be shown that a metal-insulator transition occurs if the the ratio U/t is increased.

The Hubbard model for the one-dimensional chain considering nearest neighbor hopping is given by

$$\mathcal{H}_H = -t \sum_{i,\sigma} (c_{i\sigma}^{\dagger} c_{i+1\sigma} + c_{i+1\sigma}^{\dagger} c_{i\sigma}) + U \sum_{i} n_{i\uparrow} n_{i\downarrow}. \tag{2.17}$$

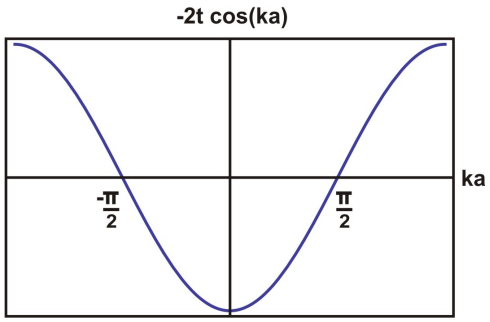

Figure 2.1: The free electron energy $\epsilon_k = -2t\cos(ka)$ for $-\pi < ka < \pi$

The Fourier transform to momentum space for the creation and annihilation operator is defined as

$$c^\dagger_{\mathbf{k}\sigma} = \frac{1}{\sqrt{L}} \sum_i e^{i\mathbf{k}\cdot\mathbf{X}_i} c^\dagger_{i\sigma} \tag{2.18}$$

$$c_{\mathbf{k}\sigma} = \frac{1}{\sqrt{L}} \sum_i e^{-i\mathbf{k}\cdot\mathbf{X}_i} c_{i\sigma}, \tag{2.19}$$

where $\mathbf{k}$ is the wave vector and $L = Na$ is the length of the chain. Taking the Fourier transform of the Hamiltonian for the one dimensional chain gives

$$\mathcal{H} = \sum_{k\sigma} \epsilon_k c^\dagger_{k\sigma} c_{k\sigma} + \frac{U}{L} \sum_{kk'q\neq 0,\sigma} c^\dagger_{k-q\sigma} c^\dagger_{k'+q,-\sigma} c_{k',-\sigma} c_{k\sigma}. \tag{2.20}$$

Here $\epsilon_k = -2t\cos(ka)$ is the free electron energy plotted in Fig. 2.1. The total number of electrons can be found by summing over all states with a wavevector smaller then the Fermi wavevector

$$N_e = 2 \sum_{|k|<k_f} 1 = \int_{-k_f}^{k_f} \frac{Ldk}{\pi} = \frac{2k_f}{\pi} L. \tag{2.21}$$

Note that the factor two comes from the spin degeneracy. It follows from this expression, that when the average electron number per site $N_e/N = 1$ (half filling), the Fermi wavevector $k_f = \pi/2a$. This can also be seen from Fig. 2.1. In the case of half filling the lowest energy state occurs when all negative energy states are filled. This corresponds to wave vectors for which $|k| \leq \pi/2a$.

2.2.1 Metallic state $|t| >> U$

When there is no on-site Coulomb repulsion $U = 0$, the Hubbard model reduces to the tight-binding model. The electrons can move through the material and there is no energy loss due to the double occupation of sites. Narrow bands are

formed since the electronic orbitals of neighboring atoms overlap. In this case the electrons are delocalized and the system is in a metallic state. The total kinetic energy due to hopping can be easily calculated

$$E_{kin} = 2 \sum_{|k<k_f|} \epsilon_k = -\frac{2tL}{\pi} \int_{-k_f}^{k_f} dk \cos(ka) = -\frac{4tN}{\pi}. \tag{2.22}$$

Note that the Fermi wavevector of the half filled chain is used here. If there is on-site Coulomb interaction, there will be an energy loss due to the double occupation of sites in the metal. An estimation of this energy loss can be made by using the Hartree approximation. It is assumed that the occupation of a certain site by a spin-up electron, is independent of the occupation of that site by a spin-down electron. If there are equal numbers op spin-up and spin-down electrons, the average occupation of a site by a-spin σ electron $< n_{i\sigma} >= 1/2$. The average energy loss due to the Coulomb energy is then

$$E_{cou} = U < \sum_i n_{i\downarrow} n_{i\uparrow} >= U \sum_i < n_{i\downarrow} >< n_{i\uparrow} >= \frac{UN}{4}. \tag{2.23}$$

Therefore the total energy of the metallic state is given by

$$E_{met} = -\frac{4tN}{\pi} + \frac{UN}{4}. \tag{2.24}$$

2.2.2 Antiferromagnetic insulator $U >> |t|$

If the hopping amplitude $t = 0$, the system will have no kinetic energy gain, since the electrons do not hop. The electrons are localized and the system is in an insulating state. The lowest-energy state at half filling corresponds to the state where each site contains one localized electron with either spin-up or spin-down. In this case there is no energy loss due to Coulomb interactions and the total energy is

$$E_{ins} = 0. \tag{2.25}$$

If the hopping amplitude is small compared to the strength of the Coulomb interaction ($U >> t$), electrons are allowed to hop to neighboring sites but double occupation of a site costs a lot of energy. Because of the Pauli principle, the hopping is not allowed if the neighboring site is occupied by an electron with parallel spin. The energy is thus lowered when neighboring electrons have antiparallel spins. Applying second order perturbation theory in t, the Hamiltonian in Eq. (2.17) reduces to the Heisenberg model

$$\mathcal{H}_H = -\sum_{<i,j>} J(\mathbf{s}_i \cdot \mathbf{s}_j - \frac{1}{4}), \tag{2.26}$$

where

$$J = -\frac{4t^2}{U}. \tag{2.27}$$

Here $\mathbf{s}_i$ is the spin of the electron at the site i. The energy is thus lowered by a factor J if nearest-neighbor electrons have antiparallel spins. Therefore, the ground state of the system is now the state where each site contains one electron and nearest-neighbor electrons have antiparallel spins. This antiferromagnetic ground state is shown in Fig. 2.2.

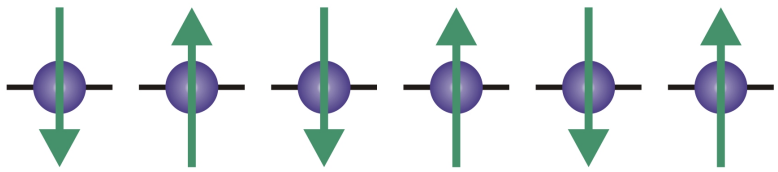

Figure 2.2: Antiferromagnetic ground state for the one-dimensional chain. The green arrows denote the electron spins.

2.2.3 Mott transition

The expression for the energy of the metallic state (Eq. 2.24) becomes positive when $U > 16t/\pi$. The system in this case will favor the insulating ground state where each site is occupied by one localized electron, since it has a lower energy (Eq. 2.25). Therefore, a metal-to-insulator transition occurs at the critical value $U_c = 16t/\pi$. This transition resulting from electron correlations is called a Mott transition. To obtain this result, we used a rather crude Hartree approximation. In general, the occupation of a certain orbital by a spin-up electron is correlated with the occupation of that orbital by the spin-down electron, and therefore, $< n_{i\uparrow} n_{i\downarrow} > \neq < n_{i\uparrow} >< n_{i\downarrow} >$.

For the one-dimensional chain an exact mathematical solution can be obtained using the nested Bethe Ansatz method. The method is very complex and does not always lead to the desired physical quantities. The exact solution at zero temperature for a half filled one-dimensional chain predicts a Mott transition for infinitesimal U.

For a one dimensional-chain special processes are important. In a free electron gas the total momentum is conserved when two electrons interact. In the case of a lattice however the total momentum modulo a reciprocal lattice vector has to be conserved. When for example two electrons with initial wave vectors $\mathbf{k}_1$ and $\mathbf{k}_2$ interact and acquire momenta $\mathbf{k}_1'$ and $\mathbf{k}_2'$, it is possible that $\mathbf{k}_1'$ lies outside the first Brillioun zone. The wavevector $\mathbf{k}_1'$ then corresponds to some wavevector within the first Brillioun zone by definition of the reciprocal space. These phenomena are called Umklapp processes. In Fig. 2.3 an example of an Umklapp process is shown. Two electrons located close to $-k_f$ scatter of two holes located around $-k_f + \frac{\pi}{2a}$. In the case $N_e < N$ (left), this process costs alot

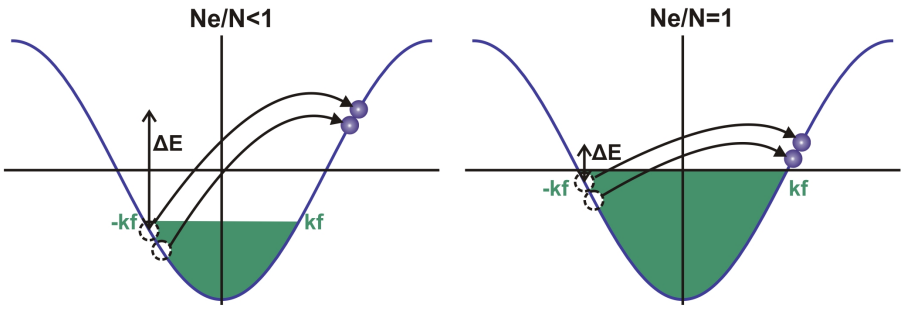

Figure 2.3: Umklapp process for $N_e/N < 1$ (left) and for $N_e/N = 1$. Two electrons located at -k_f scatter of two holes located at $-k_f + \frac{\pi}{a}$.

of energy. However in the half filling case $k_f = \frac{\pi}{2a}$ (right), the process hardly costs any energy.

The Hubbard model can describe the Mott transition. When the Coulomb interaction is small, the electrons travel through the material easily. When the Coulomb interaction is stronger it is energetically favorable for the system to localize electrons and the system becomes an insulator. For higher dimensional systems ($d > 1$) an exact solution of the Hubbard model does not exist. Mean field theories or other techniques are, therefore, needed. The Hartree approximation is a static mean field theory, where quantum- and spatial fluctuations are neglected. This is an oversimplified theory and cannot describe the Mott transition properly.

2.3 Mott transition for V_2O_3

There are two different types of Mott transitions. First of all one can change the strength of the interaction parameters t and U and obtain the transition. The transition can also be obtained by keeping the interaction parameters constant, but change the filling by doping the system. This is for example done in high temperature superconductors, which are namely doped Mott insulators. In this report the Mott transition for the honeycomb lattice at half filling will be studied by changing the interaction strengths.

The Mott transition has been observed in many transition metal oxides like for instance V_2O_3. The U/t ratio can be changed in experiments, for example by applying a pressure. Applying a pressure decreases the lattice constant and, therefore, increases the hopping amplitude t. In Fig. 2.4 an experimental phase diagram[1] of V_2O_3 is shown as a function of temperature, pressure and doping

[1] McWhan et al. Phys. Rev. B. volume 7 number 5 (1973)

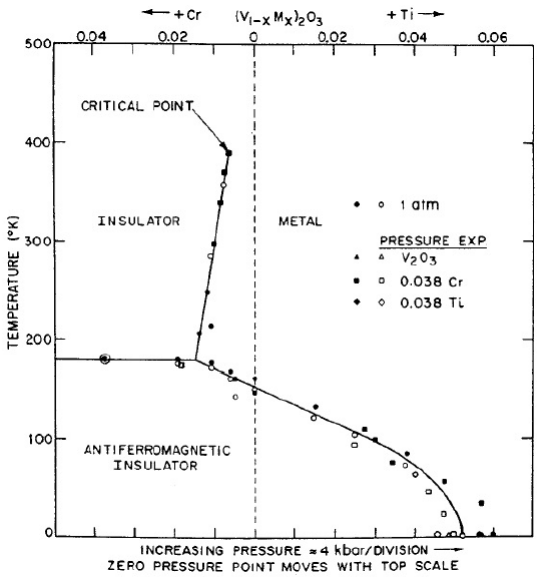

Figure 2.4: Experimental phase diagram showing the metal-insulator transition in V_2O_3 as a function of temperature, pressure and doping with Cr or Ti.

with Cr an Ti. The pressure and doping can decrease the lattice constant and thus increase the hopping amplitude. All phase transitions shown in the diagram are of first order.

At low temperatures and low (negative) pressure, V_2O_3 is in an antiferromagnetic insulating state. This is comparable to the situation for the antiferromagnetic one-dimensional chain shown in Fig. 2.2. When the temperature is increased a transition occurs to a paramagnetic insulating state which is accompanied by a change in crystal symmetry. The system however is still in an insulating state. When the pressure is increased, the factor U/t is decreased and the system undergoes a phase transition to a metallic state for both insulating states. This is a clear example of a Mott transition.

An important modern experimental technique in the study of strongly correlated electrons systems is angle-resolved photo emission spectroscopy (ARPES). In these experiments $A(\mathbf{k},\omega)f(\omega)$ is measured. Here $A(\mathbf{k},\omega)$ is the probability for an electron to have wavevector $\mathbf{k}$ and frequency ω, also called the spectral weight and $f(\omega)$ is the Fermi-Dirac function

$$f(\omega) = \frac{1}{e^{(\hbar\omega-\mu)/k_BT}+1}. \tag{2.28}$$

It is difficult to calculate the spectral weight for strongly correlated electron systems. The spectral weight, however, can be compared to the experimentally

obtained results of the ARPES experiments, which have increased resolution over the past years.

2.4 Landau-Fermi liquid theory

Different methods have been developed historically, which can describe (parts) of the phase diagram for V_2O_3. Hubbard described the paramagnetic insulator-metal transition by stating that there are two separated bands for large values of the Coulomb interaction U. If the Coulomb interaction would be reduced, the bands would move closer together and at some point overlap. The system would then be in a metallic state.

A different description of the Metal-Insulator transition uses Landau Fermi-liquid theory. A Fermi liquid has a Fermi wavevector $\mathbf{k}_f$. At sufficiently low temperatures all single particle states with wavevector $\mathbf{k} < \mathbf{k}_f$ will be occupied and states with wavevector $\mathbf{k} > \mathbf{k}_f$ are empty. The system can be excited by adding a particle with wavevector $\mathbf{k} > \mathbf{k}_f$ or by creating a hole by removing one of the particles. Landau Fermi-liquid theory assumes a one-to-one correspondence between the states of a free Fermi gas and the states of the interacting system. This means that if one starts in the grounds state of a free Fermi system and then adiabatically increases the interaction between particles, one ends up in the ground state of the interacting Fermi system. The particles in the interacting system have the same momentum and spin as the particles in the free Fermi gas but their dynamical properties like their mass is different. Excitations in the interacting Fermi liquid are called quasiparticles. These quasiparticles do not describe the motion of a single particle but also describe how a particle affects its environment. Therefore, it describes the motion of many particles. The quasiparticles have a well defined effective mass, effective interactions and a finite life time.

Since the particles in a Fermi liquid interact, there can exist collective modes. In the free Fermi gas, however, there is no interaction, so there are no corresponding states to the collective modes in the Fermi liquid. The one-to-one correspondence is, therefore, not valid in general. The contribution of the collective modes at sufficiently low temperatures can, however, be neglected for many systems. This does not apply to superconductors and superfluids, where bound states are important. In the region of low temperatures Landau Fermi-liquid theory is powerful in studying systems with interacting fermions.

Brinkman and Rice described the metallic state by a strongly correlated Fermi-liquid. If the interaction U between particles increases the effective mass m^* of the quasiparticles increases. At some critical value for U the quasiparticle residue $Z = m/m^* \to 0$ and the quasiparticles are localized. The disappearance (localization) of the quasiparticles marks the Mott transition to an insulating state. The Landau Fermi-liquid theory is a low energy approach and, therefore,

does not take into account the high-energy Hubbard bands. It, therefore, can not give an accurate description of the insulator, which consists of two Hubbard bands.

2.5 Conclusion

Transition metal oxides have partially filled d shells, which are formed by atomic orbitals. The orbitals are narrow and, therefore, the spatial extend of the orbitals is small. The smaller the spatial extend, the longer is the average time that an electron occupies a certain orbital and the more it feels the presence of other electrons at that orbital. Electron correlations are, therefore, important in transition metal oxides and give rise to interesting phenomena, such as the Mott transition.

The Hubbard model is a tight-binding model extended with Coulomb interactions between electrons and can be used to describe the Mott transition. It is however difficult to solve the Hubbard model, because of the large number of particles and the two-body Coulomb interaction term. For dimensions $d > 1$, an exact solution for the Hubbard model no longer exists. Static mean field theories like the Hartree(-Fock) approximation can be used to solve the Hubbard model but are oversimplified. In general, the density of particles at a position $\mathbf{x}$ is influenced by the density of particles at a position $\mathbf{x}'$ and $< n(\mathbf{x})n(\mathbf{x}') > \neq < n(\mathbf{x}) >< n(\mathbf{x}') >$.

Different techniques are thus needed in to describe electron correlations properly and to study the Mott transition. In the limit of infinite spatial dimensions an exact technique exists, which is called Dynamical Mean Field Theory. It is a mean field theory that takes into account quantum fluctuations. This technique will be studied in the next chapter.

Chapter 3

Dynamical Mean Field Theory Formalism

It is difficult to describe many body systems where electron correlations are important. The strength of the Coulomb interaction in these systems is comparable to the kinetic energy and, therefore, perturbation theory does not apply. Other difficulties arising in describing these systems, are for instance spatial- and quantum fluctuations and long range order. The Hubbard model cannot be solved analytically for systems with dimension two or larger. Therefore, numerical techniques are needed.

The technique studied in this chapter is called the local impurity self-consistent approximation. It is a mean field theory, which shows a great analogy with the Weiss mean field theory used for the Ising model in statistical mechanics. Instead of studying the entire lattice, one looks at a single quantum impurity site which is placed in an effective medium (mean field). The single impurity site can exchange electrons with the effective medium so that on-site quantum fluctuations are taken into full account. The system is described by a self-consistent set of equations, which include the translational invariance of the lattice. Because of the possibility for temporal change in quantum states, the local impurity self-consistent approximation is also called dynamical mean field theory (DMFT). DMFT becomes exact in the limit of non-interacting electrons $U = 0$, and like the Ising model, in the limit of infinite lattice coordination.

This chapter starts by looking at the Hubbard model in infinite dimensions. In this limit the Hubbard model reduces to a single impurity site problem. The self consistent equations describing the single impurity site in the medium will be derived. We will use iterative perturbation theory to solve the set of equations. As an example, the theory is applied to a Bethe lattice. The density of states for different ratios of the interaction parameters U/t, is calculated, which are used to study the Mott transition. Green's functions play an important role

in DMFT and a brief discussion on them can be found in Appendix A.

3.1 Hubbard model in infinite dimensions.

Here the Hubbard model in infinite spatial dimensions is described. In this limit DMFT becomes exact.

3.1.1 Density of states for hypercubic lattice

For the Hubbard model the Coulomb interaction is only nonzero if two electrons are located at the same site. It is a local quantity and does not depend on the structure of the lattice. The Coulomb interaction term is thus not affected by the limit of infinite lattice coordination (dimensions). Therefore, we only look at the kinetic energy term of the Hubbard model in this section.

The density of states of a system depends on the structure of the lattice. Here a hypercubic lattice in d dimensions is considered. For a hypercubic lattice each site has two nearest neighbors for each dimension ($z = 2d$). In Fig. 3.1 the hypercubic lattice is depicted for $d = 1$ (one dimensional chain), $d = 2$ (square lattice) and $d = 3$ (cubic lattice). Only nearest neighbor interaction is taken into account and the lattice constant in every direction is taken equal to unity. The kinetic energy of an electron with wavevector $\mathbf{k} = (k_1, k_2, ..., k_d)$ is given by

$$\epsilon_k = -2t \sum_{n=1}^{d} \cos(k_n). \tag{3.1}$$

In the limit that $d \to \infty$, the hopping amplitude has to be rescaled to $t \to \frac{t}{\sqrt{2d}}$, in order to keep the kinetic energy of the system finite. The rescaling is also necessary to keep the width of the density of states independent of the dimension, which we will show here. The kinetic energy includes the rescaling from now on

$$\epsilon_k = -\frac{2t}{\sqrt{2d}} \sum_{n=1}^{d} \cos(k_n). \tag{3.2}$$

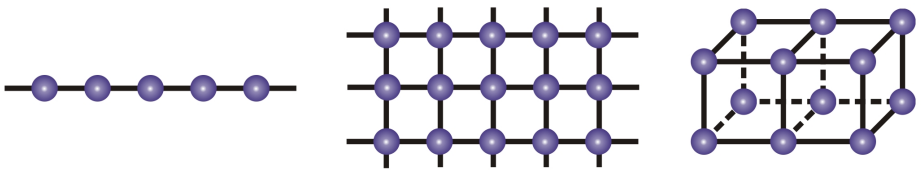

Figure 3.1: The hypercubic lattice for d=1 (one dimensional chain), d=2 (square lattice) and d=3 (cubic lattice).

The density of states in the case of non-interacting electrons ($U = 0$) is by definition:

$$\rho_0(\epsilon) = \sum_{\mathbf{k}} \delta(\epsilon - \epsilon_{\mathbf{k}}) = \prod_{n=1}^{D} \int_{-\pi}^{\pi} \frac{dk_n}{2\pi} \delta(\epsilon - \epsilon_{\mathbf{k}}). \tag{3.3}$$

Taking the Fourier transform with respect to ϵ gives

$$\rho_0(s) = \int_{-\infty}^{\infty} \rho_0(\epsilon) e^{is\epsilon} d\epsilon = (\int_{-\pi}^{\pi} \frac{dk}{2\pi} e^{-i\frac{2t}{\sqrt{2d}} s\cos(ka)})^d = (J_0(\frac{2t}{\sqrt{2d}} s))^d. \tag{3.4}$$

Here $J_0(x)$ is the zeroth order Bessel function which has its maximum value around $x = 0$. Since the Bessel function is taken to the power d, which is very large, the main contribution to the integral comes from the region $s = 0$. Expanding the integrand and performing the integral over k leads to

$$\rho(s) = e^{-\frac{1}{2}t^2 s^2 - \frac{1}{16d} t^4 s^4 + O(\frac{1}{d^2}))}. \tag{3.5}$$

In the limit of infinite dimensions $d \to \infty$ only the first term in the exponent matters. Performing the inverse Fourier transform with respect to s results in a Gaussian density of states

$$\rho(\epsilon) = \frac{1}{\sqrt{2\pi t^2}} e^{-\frac{\epsilon^2}{2t^2}}. \tag{3.6}$$

If the hopping amplitude would not have been rescaled the density of states would read

$$\rho(\epsilon) = \frac{1}{\sqrt{4\pi dt^2}} e^{-\frac{\epsilon^2}{4dt^2}}. \tag{3.7}$$

The width of this density of states would increase with increasing dimension, which is unphysical. The Gaussian density of states in Eq. 3.6 does not contain any singularities. In Fig. 3.2 the density of states for the hypercubic lattice for different dimensions is shown[1]. The lower-dimensional density of states have van Hove singularities, which originate from local maxima of the zeroth order Bessel function. The contribution of these local maxima is however of order e^{-d}, and thus vanishes for large dimensions. The local maxima did not contribute to the Gaussian density of states (Eq. 3.6) because of the expansion around $s = 0$. It can be seen from the figure that the infinite dimension solution is approached well by even low-dimensional ($d = 2, 3$) density of states plots.

The Hubbard model in the limit of infinite dimensions including the rescaling of the hopping amplitude is given by

$$\mathcal{H}_H = -\frac{t}{\sqrt{2d}} \sum_{<ij>,\sigma} c_{i\sigma}^\dagger c_{j\sigma} + U \sum_i n_{i\uparrow} n_{i\downarrow}. \tag{3.8}$$

[1] D. Vollhardt *Dynamical Mean Field Theory of Electronic Correlations in Models and Materials*, (2010)

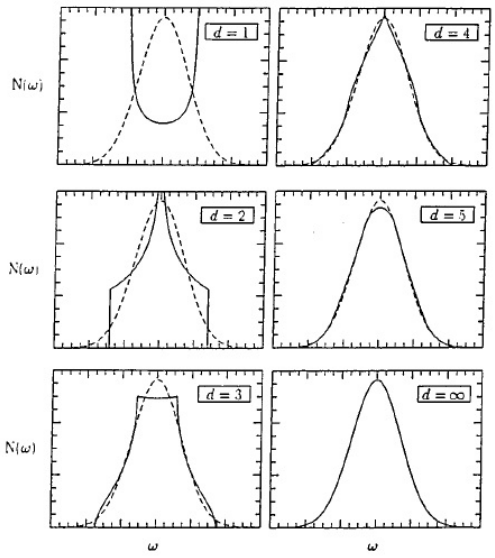

Figure 3.2: The density of states $\rho_0(\epsilon)$ for the hypercubic lattice for different dimensions $d = 1, 2, 3, 4, 5, \infty$. The infinite dimensional Gaussian density of states is shown by a dashed line.

The Coulomb interaction and kinetic energy term are of the same order of magnitude here, because of the rescaling. The Hamiltonian, therefore, keeps all the interesting physics of the Hubbard model (Eq. 2.15). The limit of infinite dimension does, however, lead to a simplification which will be shown in the next subsection.

3.1.2 Self-energy

Green's functions are used in this report to study electron correlations. We define $\psi^\dagger_\sigma(\mathbf{r}, t)$ ($\psi_\sigma(\mathbf{r}, t)$) as the creation (annihilation) operator of a spin projection σ electron, at the time t and position $\mathbf{r}$. The one-particle Green's function can be defined as

$$\mathcal{G}(\mathbf{r}, t, \mathbf{r}', t') = -i < \Phi_0 | T_t(\psi_\sigma(\mathbf{r}, t)\psi^\dagger_\sigma(\mathbf{r}', t')) | \Phi_0 >, \tag{3.9}$$

where Φ_0 denotes the ground state of the system and T_t is the Dyson time-ordered product

$$T_t(\psi_\sigma(\mathbf{r}, t)\psi^\dagger_\sigma(\mathbf{r}', t')) = \begin{cases} \psi_\sigma(\mathbf{r}, t)\psi^\dagger_\sigma(\mathbf{r}', t') & \text{if } t' < t \\ -\psi^\dagger_\sigma(\mathbf{r}', t')\psi_\sigma(\mathbf{r}, t) & \text{if } t > t'. \end{cases} \tag{3.10}$$

For $t > t'$, the one-particle Green's function in Eq. (3.9) describes the propagation of an added electron to the system, from the coordinate $\mathbf{r}'$ to the coordinate

$\mathbf{r}$ in a time $t - t'$. For $t < t'$ the Green's function describes the propagation of a hole. In order to lighten notation t' and r' can be taken equal to zero, so that

$$\mathcal{G}(\mathbf{r}, t, \mathbf{0}, 0) = \mathcal{G}(\mathbf{r}, t) \tag{3.11}$$

For non-interacting electrons the Hubbard model reduces to the tight-binding model. Taking the Fourier transform with respect to time and with to momentum space, the one-particle Green's function for the tight-binding model can be written as (see Appendix A.1)

$$G^0_{\mathbf{k}}(\omega) = \frac{1}{\omega + \mu - \epsilon_{\mathbf{k}}}, \tag{3.12}$$

where $\mathbf{k}$ is the wavevector, ω is the frequency, μ is the chemical potential and $\epsilon_{\mathbf{k}}$ is the dispersion. Coulomb interactions between electrons can be taken into account via the self energy $\Sigma_\sigma(\mathbf{k}, \omega)$, which in general is a function of the electron spin, wavevector and frequency. The one-particle propagator including electron-electron interactions can be written as

$$G_{\mathbf{k}\sigma}(\omega) = \frac{1}{\omega + \mu - \epsilon_{\mathbf{k}} - \Sigma_\sigma(\mathbf{k}, \omega)}. \tag{3.13}$$

The self-energy is a matrix in site labels i and j since it is a function of the wavevector

$$\Sigma_{\sigma,ij}(\omega) = \frac{1}{L} \sum_{\mathbf{k}} \Sigma(\mathbf{k}, \omega) e^{i\mathbf{k}\cdot(\mathbf{R}_i - \mathbf{R}_j)}. \tag{3.14}$$

The lowest-order diagram for the self-energy connecting the sites i and j is shown in Fig. 3.3 and involves the hopping between the two sites three times. In the infinite dimensional Hubbard model, a rescaling of the hopping amplitude

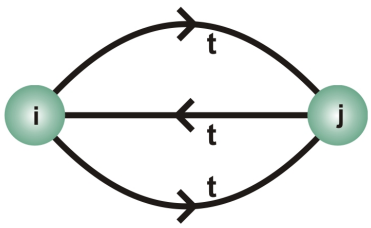

Figure 3.3: Lowest order diagram for the self energy between sites i and j.

$t/\sqrt{2d}$ is necessary as described in the previous subsection. An off-diagonal term of the self-energy $\sum_{ij}$ (where $i \neq j$) is therefore smaller by a factor $(1/2d)^{3/2}$ then a diagonal term, which does not contain the hopping amplitude. For the hypercubic lattice, each site has $2d$ nearest neighbors. Therefore, if only nearest neighbor interaction is considered, there are $2d$ nonzero off diagonal elements for each diagonal element in the self-energy matrix. The contribution

of the off-diagonal elements is thus smaller by a factor $1/\sqrt{2d}$ compared to the diagonal elements. In the limit of infinite dimensions the off-diagonal terms can, therefore, be neglected and the self-energy is independent of the wavevector

$$\lim_{d\to\infty} \Sigma(\omega, \mathbf{k}) = \Sigma(\omega). \tag{3.15}$$

At zero temperature the chemical potential is equal to the Fermi energy E_f. The Fermi surface is by definition the surface for which the denominator of the one particle propagator (Eq. 3.13) is equal to zero for $\omega = 0$. This leads to the equation

$$\epsilon_{\mathbf{k}} + \Sigma(\mathbf{k}, 0) = E_f. \tag{3.16}$$

The Fermi surface in the case of non-interacting electrons ($\Sigma(\mathbf{k}, \omega) = 0$) is expected to be very different from the Fermi surface when the electrons do interact. When the self-energy is independent of $\mathbf{k}$, the Fermi energy is only shifted from the non-interacting value by $\Sigma(0)$. The Fermi surface and the volume it encloses, however, are unchanged.

Neglecting the $\mathbf{k}$-dependence of the self-energy simplifies the study of strongly correlated electron systems, which will be shown in the next section.

3.2 DMFT equations

In mean field theories such as the Hartree-Fock approximation the self-energy is a static potential. However, in Dynamical Mean Field Theory the self-energy is time dependent and can describe the interactions between electrons dynamically. The electron correlations in materials lead to interesting phenomena such as the Mott transition, which can be described by DMFT. In DMFT one studies a single site impurity embedded in an effective medium (bath). The single impurity site interacting with the bath is described by a set of self-consistent equations. These equations include the translational invariance of the lattice and are exact in the limit of infinite dimensions. There are different numerical methods for solving the set of equations, such as Quantum Monte Carlo simulations and Exact Diagonalization. We will use a technique called iterative perturbation theory. In this section, equations describing the impurity site will be derived.

3.2.1 Lattice Green's function

When using Green's functions it is sometimes convenient to use the imaginary time Green's function also called Matsubara Green's function. The one-particle propagator for the imaginary time $\tau = it$ is defined as

$$\mathcal{G}_\sigma(\mathbf{k}, \tau) = - < \Phi_0 | T_\tau (c_{\mathbf{k}\sigma}(\tau) c^\dagger_{\mathbf{k}\sigma}(0)) | \Phi_0 >, \tag{3.17}$$

where T_τ denotes the time ordered product. The Green's function describes the propagation of an electron if the imaginary time $\tau > 0$, and the propagation of a hole, if $\tau < 0$. Taking the Fourier transform with respect to ω, the Green's function can be written as

$$\mathcal{G}_\sigma(\mathbf{k}, i\omega_m) = \frac{1}{i\omega_m + \mu - \epsilon_\mathbf{k} - \Sigma(\mathbf{k}, i\omega_m)}, \tag{3.18}$$

where ω_m is the Matsubara frequency. The imaginary time Green's function is an antiperiodic function with the period $\beta = 1/T$. Therefore, the Matsubara frequencies are odd $\omega_m = (2m+1)\pi T$. The inverse Fourier transform to coordinate space is given by

$$G_{\sigma,ij}(i\omega_m) = \frac{1}{L}\sum_\mathbf{k} G_\sigma(\mathbf{k}, i\omega_m) e^{i\mathbf{k}(\mathbf{R}_i - \mathbf{R}_j)}. \tag{3.19}$$

The local part of the Green's function $G_{\sigma,ii}$ can thus be calculated by summing Eq. A.18 over all wavevectors $\mathbf{k}$. The self-energy is assumed to be independent of $\mathbf{k}$, which leads to the following expression for the on-site Green's function

$$\begin{aligned}
\mathcal{G}_{\sigma,ii}(i\omega_m) &= \frac{1}{L}\sum_\mathbf{k} \frac{1}{i\omega_m + \mu - \epsilon_\mathbf{k} - \Sigma(i\omega_m)} \\
&= \int d\epsilon \sum_\mathbf{k} \frac{1}{L} \frac{\delta(\epsilon - \epsilon_k)}{i\omega_m + \mu - \epsilon - \Sigma(i\omega_m)} \\
&= \int d\epsilon \frac{\rho_0(\epsilon)}{i\omega_m + \mu - \epsilon - \Sigma(i\omega_m)}.
\end{aligned} \tag{3.20}$$

The only quantity that depends on the structure of the lattice in this expression is the density of states in the case of non-interacting electrons

$$\rho_0(\epsilon) = \frac{1}{L}\sum_\mathbf{k} \delta(\epsilon - \epsilon_\mathbf{k}). \tag{3.21}$$

The density of states for interacting electrons is given by the imaginary part of the real time Green's function

$$\rho(\omega) = -\frac{1}{\pi} Im[G_{ii}(\omega + i\eta)]. \tag{3.22}$$

Here $i\eta$ is a small imaginary number added to the real frequency to move the poles of Green's function to the lower half plane. This gives the peaks in the density of states a finite width. Since the wavevector is assumed to be independent of the wavevector, the Fermi surface does not change shape, when the Coulomb interaction between electrons is switched on. This means that the volume of the Fermi surface and, therefore, the density of particles at frequency $\omega = 0$ should also be unchanged. Since the density of states is directly related to the density of particles, the DOS at zero frequency $\rho(0)$ should be independent of electron interactions.

In this chapter imaginary time Green's functions are used. In our program for calculating the DOS a routine is needed which transforms the imaginary time Green's function to the real-time Green's function.

3.2.2 Quantum impurity model

In DMFT one does not look at the whole lattice. The Hubbard model in the limit of infinite dimensions reduces to a single-site problem, which has less degrees of freedom then the lattice model (Fig. 3.4). The single-site is embedded in

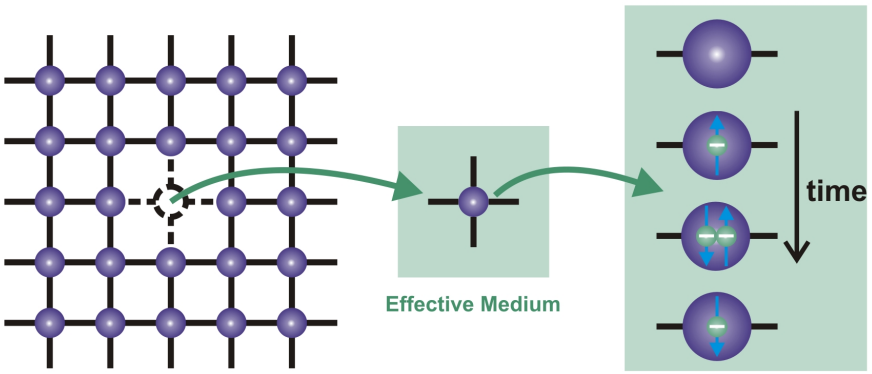

Figure 3.4: Instead of studying the whole lattice, DMFT considers a single site impurity in an effective medium. The impurity site can exchange electrons with the effective medium.

an effective medium which consist of all other particles in the lattice model. This is similar to the Weiss mean field theory used for the Ising model. In the Ising model the effective medium is a static field (magnetization) created by the nearest neighbors. In the limit of infinite lattice coordination, the fluctuations of the neighbors are unimportant and the theory becomes exact. DMFT is different from this classical mean field theory in that it allows for quantum fluctuations. The single site can exchange electrons with the bath and, therefore, can change quantum state. The effective action for the Hubbard model is given by

$$\begin{aligned} S_H &= \int_0^\beta d\tau \Big[\sum_{i\sigma} \gamma^\dagger_{i\sigma}(\tau)(\frac{\partial}{\partial\tau} - \mu)\gamma_{i\sigma}(\tau) - \sum_{ij\sigma} t_{ij}\gamma^\dagger_{i\sigma}(\tau)\gamma_{j\sigma}(\tau) \\ &\quad + \sum_i U n_{i\uparrow}(\tau) n_{i\downarrow}(\tau) \Big], \end{aligned} \tag{3.23}$$

where $\gamma^\dagger_{i\sigma}$ and $\gamma_{i\sigma}$ are Grassmann variables corresponding the annihilation $c_{i\sigma}$ and creation operator $c^\dagger_{i\sigma}$ respectively and $n_{i\sigma}(\tau) = \gamma^\dagger_{i\sigma}(\tau)\gamma_{i\sigma}(\tau)$. It can be

shown using the coherent potential approximation [10], or the cavity method [8], that the local effective action for the Hubbard model in the limit of infinite dimensions can be written as

$$\begin{aligned} S_e &= -\int_0^\beta d\tau \int_0^\beta d\tau' \sum_\sigma \gamma_\sigma^\dagger(\tau)[\mathcal{G}_\sigma^0(\tau-\tau')]^{-1}\gamma_\sigma(\tau') \\ &\quad + U\int_0^\beta d\tau n_\uparrow(\tau)n_\downarrow(\tau), \end{aligned} \tag{3.24}$$

where,

$$[\mathcal{G}_\sigma^0(\tau-\tau')]^{-1} = -(\frac{\partial}{\partial\tau}-\mu)\delta_{\tau\tau'} + \sum_{i\neq j} t_{i0}^* t_{j0}^* G_{\sigma,ij}(\tau-\tau') \tag{3.25}$$

The first term of the effective action describes the exchange of electrons between the impurity site and the rest of the lattice. It describes the possibility for an electron to be created at the impurity site at a time τ' coming from the effective medium (bath) and then at a time τ go back to the bath, and vice versa, for an electron to go to the bath at a time τ' and come back to the impurity site at a time τ. $\mathcal{G}_0(\tau-\tau')$ is called the Weiss effective field and is the amplitude for this processes to occur. The Weiss field is the bare Green's function ($U=0$) of the impurity model, which is not equivalent to the non interacting local Green's function of the lattice model. In classical mean field theory the Weiss field is represented by a number, which in fact freezes local quantum fluctuations. This approach is often only valid at low energies. In the quantum impurity model the Weiss field is a function of the imaginary time. Since the possibility for temporal change in quantum states, quantum fluctuations are taken into account. Spatial fluctuations are neglected however, since only a single site is studied. The second term in Eq. 3.24 describes the Coulomb interaction between two electrons when they occupy the impurity site at the same time.

The effective action is still a many body problem because quantum fluctuations are taken into account. The number of electrons at the impurity site continuously changes between 0,1 and 2 in time.

3.2.3 Anderson impurity model

It is convenient to have a Hamiltonian representation of the effective action Eq. 3.24 to do practical calculations. The Anderson model is often used to describe magnetic impurities in non magnetic materials and can be used to describe the impurity site embedded in the effective medium. The Hamiltonian is given by

$$\mathcal{H}_A = \sum_{\mathbf{k}\sigma}\epsilon_{\mathbf{k}}c_{\mathbf{k}\sigma}^\dagger c_{\mathbf{k}\sigma} + \sum_\sigma \epsilon_d d_\sigma^\dagger d_\sigma + U n_{d\uparrow}n_{d\downarrow} + \sum_{\mathbf{k}\sigma}[V_{kd}c_{\mathbf{k}\sigma}^\dagger d_\sigma + h.c.]. \tag{3.26}$$

Here $c_{k\sigma}^\dagger$ creates an electron with wavevector $\mathbf{k}$ in the effective medium and $d^\dagger$ creates an electron at the localized orbital at the impurity site. The first and

second term represent the kinetic energy of the electrons in the medium and localized orbital respectively. The third term represents the on-site Coulomb repulsion between two electrons when they occupy the localized orbital. The fourth term allows an electron to hop from the local orbital into the effective medium with mixing integral V_{kd} and, vice versa, to hop from the effective medium to the localized orbital. The one-particle Green's function for the non-interacting case $U = 0$ for the Anderson model is (see Appendix A.3)

$$\begin{aligned}[\mathcal{G}_\sigma^{A0}(i\omega_m)]^{-1} &= -<\Phi_0|(d_\sigma(\tau)d_\sigma^\dagger(0))|\Phi_0> \\ &= i\omega_m - \epsilon_d - \int_{-\infty}^{\infty} d\epsilon \frac{\Delta(\epsilon)}{i\omega_m - \epsilon}, \end{aligned} \tag{3.27}$$

where

$$\Delta(\epsilon) = \sum_{\mathbf{k}} |V_{\mathbf{k}}|^2 \delta(\epsilon - \epsilon_{\mathbf{k}}). \tag{3.28}$$

$\Delta(\epsilon)$ can be chosen such that the non-interacting one-particle Green's function equals the Weiss Green's function in Eq. 3.25. The Anderson model is then a Hamiltonian description of the effective action for the impurity site.

The electron interactions are taken into account via the self-energy. The first-order diagram in U results in the Hartree-Fock approximation which leads to a shift in the chemical potential ($U/2$ for half filling). The contribution of this diagram is however uninteresting to us, because we are only interested in the shape of the density of states from which we will study the Mott transition. The second order in U contribution to the self-energy is

$$\Sigma(\tau) = U^2 \mathcal{G}_0^A(\tau)\mathcal{G}_0^A(\tau)\mathcal{G}_0^A(-\tau). \tag{3.29}$$

This corresponds to the diagram shown in Fig. 3.5. The added electron for the Green's function scatters of another electron of the system creating an electron hole pair at time $\tau = 0$. The electron then propagates and scatters again at a time $\tau = t$ and the electron-hole pair is destroyed. The self-energy of the on site lattice Green's function in Eq. 3.20 is a local quantity. Therefore, the self-energy of the Anderson impurity model describing the single site is assumed to

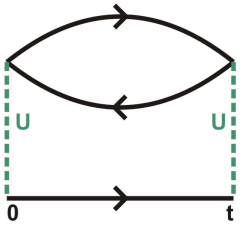

Figure 3.5: The second order in U self energy diagram.

be equal to the self-energy of the lattice Green's function. The Dyson equation then links the interacting lattice Green's function to the non-interacting Green's function of the impurity model via the self-energy

$$G_{00,\sigma}(i\omega_m) = \frac{1}{[\mathcal{G}^{A0}_\sigma]^{-1} - \Sigma(i\omega_m)}. \tag{3.30}$$

The equations for the lattice Green's function 3.20, bare Green's function of the impurity model 3.27, self-energy 3.29 and the Dyson equation now form a self-consistent set.

3.2.4 Iterative perturbation theory

A method for solving the set of equations is iterative perturbation theory (IPT). It is a perturbation theory because self-energy diagrams to second order in U are considered. It might doubtful whether perturbation theory is still valid for large values of U, in which we are interested. We return to this question later.

The procedure for the IPT calculation is shown in Fig. 3.6. First the Coulomb interaction $U = 0$. The calculation starts by making an educated guess for the non-interacting Green's function of the impurity model. From this function the self-energy is easily calculated using Eq. 3.29. The lattice Green's function is then calculated using Eq. 3.20. For this the non-interacting density of states $\rho_0(\epsilon)$ is needed which is calculated prior to the IPT. Depending on the DOS the integral in Eq. 3.20 can be calculated either exactly before the IPT or numerically during the IPT routine. Using the Dyson equation the non-interacting Green's function of the impurity model is calculated and cycle starts again. The iteration stops when the lattice Green's function has converged (does not change values after another cycle). The value of the Coulomb interaction is increased to $U + \delta U$ and the iteration continues using the just obtained lattice Green's function as an initial value. This procedure is repeated until the lattice Green's function is obtained for the desired value of the Coulomb interaction strength.

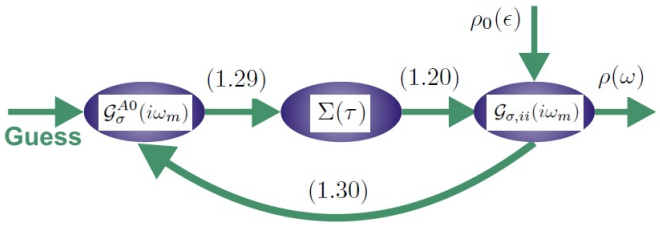

Figure 3.6: Schematic diagram for iterative perturbation theory. The numbers denote the equations used to calculate the next step.

After the IPT the lattice Green's function is a function of imaginary Matsubara frequencies $i\omega_m$. Padé approximants are used to transform the Green's function to real frequencies. The density of states is then obtained by taking the imaginary part of the real ω lattice Green's function (Eq. 3.22).

3.3 Mott transition on Bethe lattice

We want to study the Mott transition on a lattice by calculating the density of states for different values of U/t. One of the advantages of DMFT is that it is valid for all interaction strengths U, t, and temperatures. For a hypercubic lattice an infinite Coulomb interaction strength is needed to realize a Mott transition, since the non-interacting Gaussian density of states (Eq. 3.6) has a finite value for infinite energies. In real materials the density of states, however, is confined to a finite energy range.

To illustrate the iterative perturbation theory method, the Mott transition for the Bethe lattice shown in Fig. 3.7 at half filling is studied here. The only quantity needed in the method that depends on the structure of the lattice is the non-interacting density of states. In the limit of infinite dimension the Bethe lattice has a semicircular density of states

$$\rho_0(\epsilon) = \frac{2}{\pi D^2}\sqrt{D^2 - \epsilon^2}, \tag{3.31}$$

where $D = 2t$ is the half-bandwidth. For each cycle in the iterative perturbation theory the local Green's function has to be calculated by solving the integral in Eq. 3.20. Substituting the expression for the semicircular density of states into this equation gives

$$\mathcal{G}_{00,\sigma}(i\omega_m) = \frac{2}{\pi D^2}\int_{-D}^{D} d\epsilon \frac{\sqrt{D^2 - \epsilon^2}}{i\omega_n + \mu - \epsilon + \Sigma(\omega)}. \tag{3.32}$$

This integral can be calculated using Cauchy's residue theory (See Appendix B). The result is

$$\mathcal{G}_{00,\sigma}(i\omega_m) = \left\{ \begin{array}{ll} \frac{2}{\nu(i\omega_m)+\eta(i\omega_m)\sqrt{\nu(i\omega_m)^2-4t^2}} & (\eta(i\omega_m) = \pm 1) \\ \frac{\nu(i\omega_m)}{2t^2} & (\eta(i\omega_m) = 0) \end{array} \right\}, \tag{3.33}$$

where

$$\nu(i\omega_m) = i\omega_m + \mu - \Sigma(i\omega_m)$$

$$\eta(i\omega_m) = \left\{ \begin{array}{ll} 0 & \mathrm{Im}(\nu(i\omega_m)) = 0 \text{ and } |\mathrm{Re}(\nu(i\omega_m))| \leq 2t \\ +1 & \mathrm{Im}(\nu(i\omega_m)) > 0 \text{ or } \mathrm{Im}(\nu(i\omega_m)) = 0 \text{ and } \mathrm{Re}(\nu(i\omega_m)) < -2t \\ -1 & \mathrm{Im}(\nu(i\omega_m)) > 0 \text{ or } \mathrm{Im}(\nu(i\omega_m)) = 0 \text{ and } \mathrm{Re}(\nu(i\omega_m)) > 2t \end{array} \right.$$

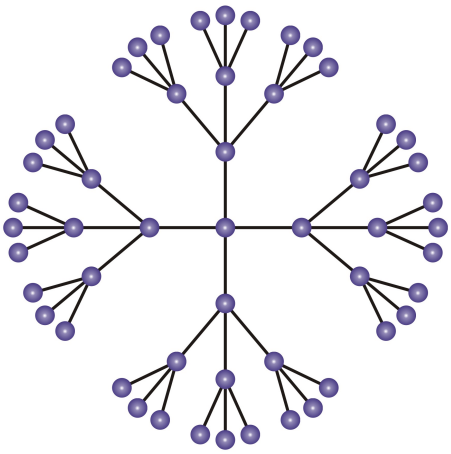

Figure 3.7: Part of the Bethe lattice with $z = 4$.

The density of states for different interaction strengths U/D obtained by IPT for the Bethe lattice at half filling is shown in Fig. 3.8. The temperature in units of the half-bandwidth was taken as $\beta D = D/T = 40$.

When the Coulomb interaction is small ($U/D = 0, 1$), the electrons are almost free and the DOS has the shape of a metal. When the Coulomb interaction is increased a typical three peak structure arises ($U/D = 2$). The system has the DOS of a strongly correlated metal. The two peaks located at $\pm U/2$ ($\omega + \mu = 0, \omega + \mu = U$) correspond to the upper and lower Hubbard bands. The peak around $\omega = 0$ corresponds to the quasiparticles from the Landau-Fermi liquid. For $U/D = 2.5$ a similar DOS is obtained but the peak at $\omega = 0$ becomes narrower, which corresponds to a mass enhancement of the quasiparticles. Note that the height of the quasiparticle peak at $\omega = 0$ does not change height as is required if the self-energy is independent of $\mathbf{k}$. At a critical value $U_c = 2.6$ the quasiparticle peak disappears and the system is in an insulating state. The DOS for $U = 3$ has two bands. The lower band $\omega = -U/2$ is completely filled (valence band) and the upper band $\omega = U/2$ is completely empty (conduction band) in the case of half filling.

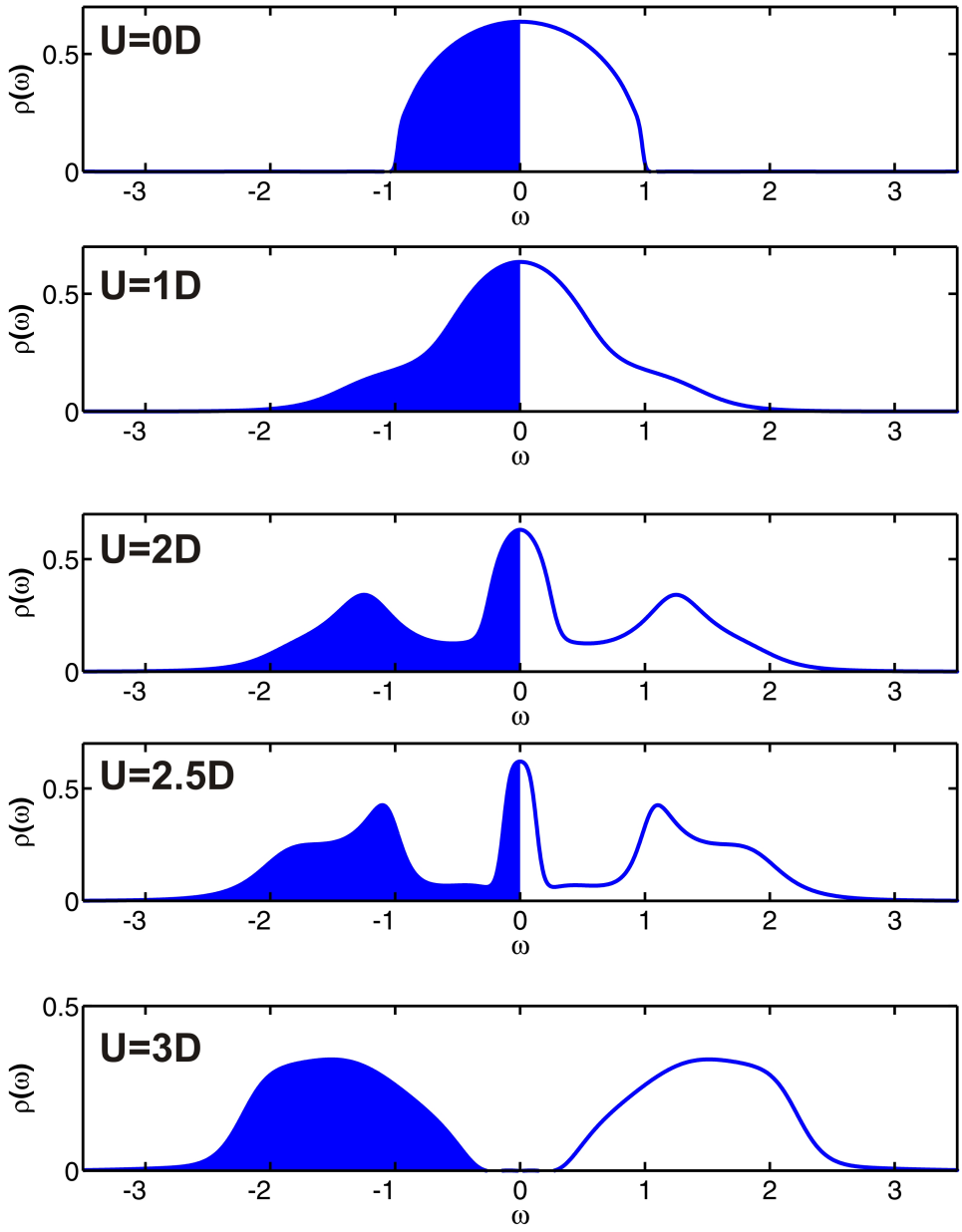

Figure 3.8: Density of states for the Bethe lattice for $U/D = 0, 1, 2, 2.5, 3$ and $\beta = 1/T = 40D$.

For the calculation of the density of states, second-order perturbation theory in the Coulomb interaction was used to calculate the self-energy. The Mott transition occurs at large values of U however, so it is questionable whether this is a good approximation. Quantum Monte Carlo simulations have been done for a semi-circular density of states in the case of non-interacting electrons by Georges *et al* [8]. The results are shown in Fig. 3.9. The QMC gives a similar result to the IPT. At low values of U, the semicircular density of states is obtained. If U is increased, the three-peak structure arises. At large values of U the quasiparticle peak disappears and the system is in an insulating state. The iterative perturbation theory, therefore, seems to be valid for large values of U.

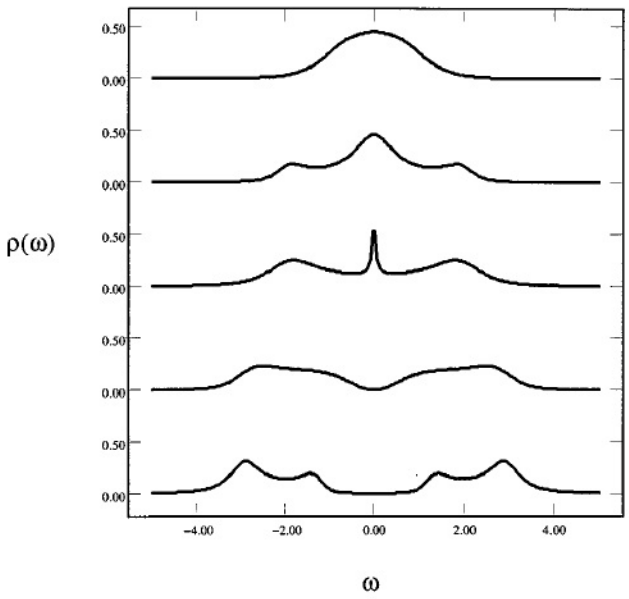

Figure 3.9: Density of states for $U\sqrt{2}/D = 1, 2, 3, 4, 5$ and $\beta D/\sqrt{2} = 10$ for the Bethe lattice using Quantum Monte Carlo simulations by [8].

Chapter 4

Mott transition for the honeycomb lattice using DMFT

Materials with a honeycomb structure show many interesting phenomena, such as the quantum spin liquid [28], and the topological Mott insulator [13]. These phenomena result from the presence of Dirac points in the corners of the first Brillouin zone. At these points the valence and conduction bands are touching and the dispersion is linear $\epsilon_{\mathbf{k}} = \pm v_F|\mathbf{k}|$, where the +(-) sign corresponds to the conduction (valence) band. The Fermi velocity v_F can be $\sim 10^6$ m/s in these systems. The particles are, therefore, described by relativistic massless Dirac fermions and the Fermi liquid theory is not applicable.

An example of a material that has a layered hexagonal structure is magnesium diboride (MgB_2). Both the magnesium- and the boron layers form a hexagonal structure. Experiments showed that MgB_2 is a phonon-mediated high-T_c superconductor [14]. The electrons in the σ-band resulting from the boron σ orbitals are expected to couple strongly to lattice vibrations (of the Boron atoms) and give rise to the superconductivity.

Another example with a hexagonal structure is graphene. Graphene consists of carbon atoms, which form a 2-d honeycomb structure that can be grown on substrates. The electronic properties of graphene depend on the environment of the 2 dimensional structure and, therefore, on the substrate. A lot of research has been done on graphene recently [15], partially motivated by possible applications in carbon based electronic devices. Graphene is a half-filled electron system. The lower band is completely filled by electrons and Dirac points are present at the Fermi energy, where the density of states vanishes. Such a system is called a semimetal. In this chapter we study the semimetal-to-insulator transition for the Honeycomb lattice using DMFT as described in

the previous chapter. For graphene the ratio of the interaction parameters [16] $U/t \approx 2.2 - 4.4$. At these values graphene is, however, still conducting.

A possible system where the interaction parameter U/t can have higher values is a two-dimensional honeycomb lattice constructed using three laser beams. A honeycomb structure can be reproduced by optically trapping ultracold atoms. The interaction parameters U/t can be changed using Feshbach resonance to regimes not obtained in graphene.

This chapter is organized as follows: First we use the tight binding model to calculate the energy dispersion $\epsilon_{\mathbf{k}}$ for the honeycomb lattice. Then the density of states will be calculated for non-interacting electrons. In Sec 3.2, the obtained density of states will be used to calculate the density of states for interacting electrons, using DMFT as described in the previous chapter. The semimetal-insulator transition will then be studied from the obtained density of states for different values of U/t.

4.1 Density of states for the tight-binding model

In this section the density of states will be calculated for non-interacting electrons on the honeycomb lattice. This DOS is needed for the DMFT method described in the previous chapter to obtain the density of states for interacting electrons. The honeycomb lattice is shown in Fig. 4.1. It is a bipartite lattice consisting of two triangular sublattices denoted by A and B. The unit cell, therefore, contains two lattice sites (one belonging to sublattice A and one belonging to sublattice B). The unit vectors are denoted by $\mathbf{a}_1$ and $\mathbf{a}_2$. The vector $\mathbf{c}$ connecting sites of the sublattices A and B has a length a(lattice constant).

4.1.1 Brillouin zone of the honeycomb lattice

The honeycomb lattice shown in figure in Fig. 4.1 has two basis vectors,

$$\begin{aligned} \mathbf{a}_1 &= (\frac{\sqrt{3}}{2}, -\frac{3}{2})a, \\ \mathbf{a}_2 &= (-\frac{\sqrt{3}}{2}, -\frac{3}{2})a. \end{aligned} \tag{4.1}$$

The reciprocal lattice can be defined by the following basis vectors [6]

$$\vec{f_1} = 2\pi \frac{\vec{a}_2 \times \vec{e}_3}{\vec{a}_1 \cdot (\vec{a}_2 \times \vec{e}_3)}, \quad f_2 = 2\pi \frac{\vec{e}_3 \times \vec{a}_1}{\vec{a}_2 \cdot (\vec{e}_3 \times \vec{a}_1)}. \tag{4.2}$$

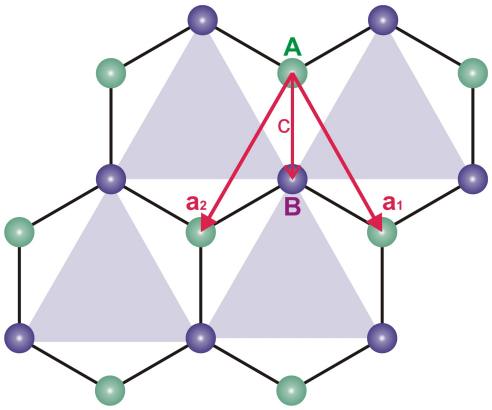

Figure 4.1: The honeycomb lattice is a bipartite lattice consisting of two triangular sublattices, which are denoted by the green and purple colors. The basis vectors of the lattice are $\mathbf{a}_1$ and $\mathbf{a}_2$.

For a two-dimensional lattice, $\vec{e}_3$ is the unit vector in the z-direction. Calculating the reciprocal lattice vectors for the honeycomb lattice gives

$$\begin{aligned} \mathbf{f}_1 &= \frac{4\pi}{3a}(\frac{\sqrt{3}}{2}, -\frac{1}{2}, 0), \\ \mathbf{f}_2 &= \frac{4\pi}{3a}(\frac{-\sqrt{3}}{2}, -\frac{1}{2}, 0). \end{aligned} \tag{4.3}$$

The reciprocal lattice of the honeycomb lattice is again a honeycomb lattice. The Brillouin zone with the Wigner-Seitz cell is shown in Fig. 4.2.

4.1.2 Calculation of the kinetic energy

In the non-interacting case $U = 0$ the Hubbard model reduces to the tight-binding model

$$\mathcal{H} = -t \sum_{<ij>} (c_i^\dagger c_j + c_j^\dagger c_i). \tag{4.4}$$

Here the spin indices are neglected, because the hopping of spin-up electrons can be treated independently from the hopping of spin-down electrons. For the honeycomb lattice a single site of the sublattice A has three nearest-neighbor sites, which are all part of the sublattice B. The Hamiltonian can be rewritten using $A_i^\dagger$ and $B_i^\dagger$ as the creation operators for an electron at the site i part of the sublattice A and B respectively:

$$\mathcal{H} = -t \sum_{<ij>} (A_i^\dagger B_j + B_j^\dagger A_i). \tag{4.5}$$

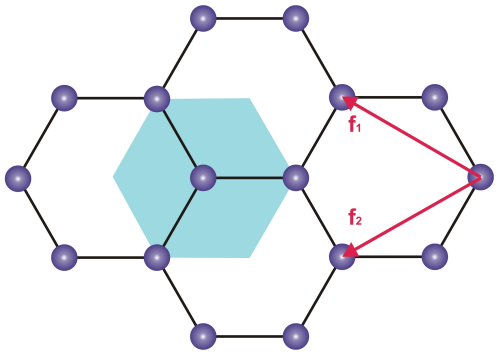

Figure 4.2: The reciprocal space of the honeycomb lattice. The Wigner Seitz cell (the first Brillouin zone) depicted by the blue surface.

Summing over all nearest neighbors and performing the Fourier transform as defined in Eq. (2.19), the Hamiltonian can be written in the following form

$$\mathcal{H} = -t \sum_{\mathbf{k}} (A_k^\dagger, B_k^\dagger) \begin{pmatrix} 0 & \epsilon_k^{ab} \\ (\epsilon_k^{ab})^* & 0 \end{pmatrix} \begin{pmatrix} A_k \\ B_k \end{pmatrix}, \tag{4.6}$$

where,

$$\epsilon_k^{ab} = e^{i(\frac{\sqrt{3}}{2}ak_x - \frac{a}{2}k_y)} + e^{i(-\frac{\sqrt{3}}{2}ak_x - \frac{1}{2}ak_y)} + e^{ik_y a}. \tag{4.7}$$

Note that the factor two in Eq. (4.6) comes from the spin degeneracy. Calculating the eigenvalues of the matrix gives the following expression for ϵ_k

$$\epsilon_k = \pm t \sqrt{1 + 4\cos^2(\frac{\sqrt{3}}{2}ak_x) + 4\cos(\frac{\sqrt{3}}{2}ak_x)\cos(\frac{3}{2}ak_y)}. \tag{4.8}$$

The function has a maximum value of $3t$ and is symmetric in k_x and k_y. The plus and minus signs correspond to the upper and lower bands. The electron dispersion is shown in Fig. 4.3[1]. At the corners of the Brillouin zone the energy is equal to zero and the upper and and lower bands touch. Close to these points the dispersion relation can be approximated by $\epsilon_{\mathbf{k}} = v_F\sqrt{\mathbf{k}_x^2 + \mathbf{k}_y^2} = v_F|\mathbf{k}|$, where v_F is the Fermi velocity and k_x and k_y are counted from the corner points here. The corners of the Brillouin zone with this linear dispersion are called Dirac points. The electrons and holes at the Dirac points have a zero mass and, therefore, behave like relativistic particles. At half-filling the lower band is completely filled and the Fermi level is shown by the red surface in Fig. 4.3.

[1] A. Giuliani *arXiv:1102.3881v1* 2011

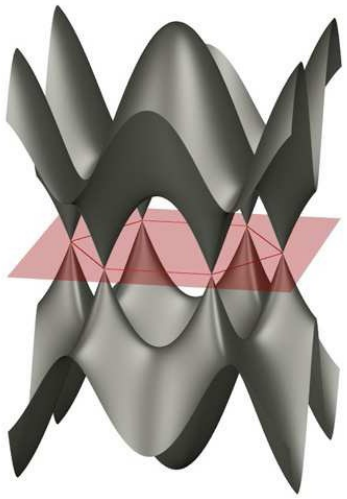

Figure 4.3: The dispersion shown for the first Brillouin zone. Dirac points are present at the corners of the Wigner-Seitz cell. The linear dispersion around these points can be clearly seen. The red surface is the Fermi energy in the case of half filling.

4.1.3 Density of states

The density of states for non-interacting electrons can be calculated using the dispersion Eq. (4.8). The density of states per spin projection for a two-dimensional lattice is by definition

$$\rho_0(\epsilon) = \frac{d}{d\epsilon}\left(\frac{1}{(2\pi)^2}\int_{\epsilon_{\mathbf{k}}<\epsilon} d^2k\right). \tag{4.9}$$

An analytical expression for $\rho_0(\epsilon)$ is given in Ref. [17]. We will calculate the density of states numerically, however. According to the expression in Eq. (4.9), we have to count the number of states within the first Brillouin zone with an energy $\epsilon_{\mathbf{k}} < \epsilon$, for different ϵ and then take the derivative with respect to ϵ. In order to count the number of states with $\epsilon_{\mathbf{k}} < \epsilon$, we can place a grid over the first Brillouin zone, shown in Fig. 4.2, and check for every point on the grid whether it has an energy $\epsilon_k < \epsilon$. The first Brillouin zone has a hexagonal structure which makes it rather inconvenient to place a grid. By symmetries however, it can be easily seen that the first Brillouin zone, can be replaced by a square shown in Fig. 4.4. The square is divided into a large number of points by placing a 10000 by 10000 grid. The energy ϵ is increased from 0 to $3.5t$ by taking 1000 steps. For each ϵ, each point on the grid is checked if it has a value smaller then ϵ. This results in an array with the number of states with $\epsilon_k < \epsilon$ as a function of ϵ. Taking the derivative with respect to ϵ and renormalizing, results in the density of states for non-interacting electrons.

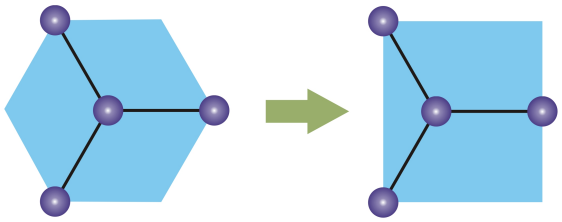

Figure 4.4: The hexagonal first Brillioun zone can be replaced by a square using the translational invariance in the **k**-space.

The resulting density of states for $t = 1/3$ is shown in Fig. 4.5. It shows the van Hove singularities at $\pm t$. The density of states vanishes at $\epsilon = 0$. In the case of half-filling, the Dirac point is located exactly at the Fermi energy. Since the gap between the upper and lower bands equals zero, the electrons near the Fermi surface can easily go to the upper band. The material is still conducting and is a so-called semimetal.

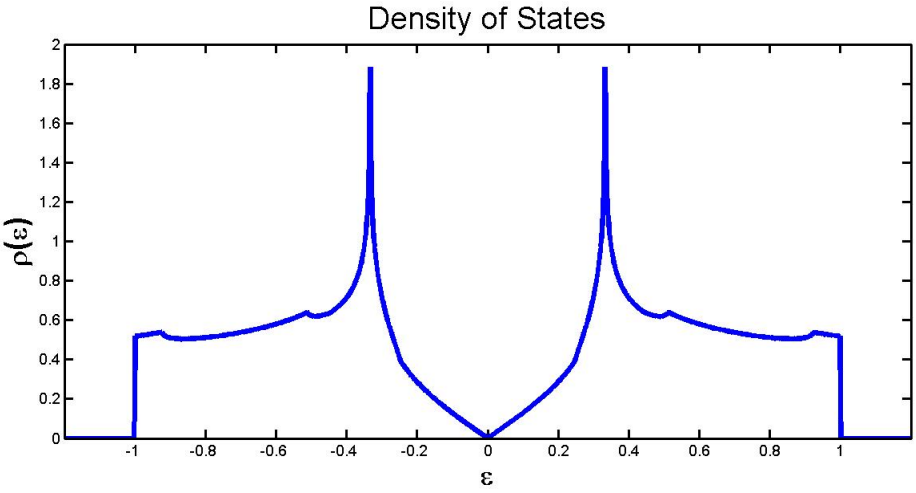

Figure 4.5: The density of states for the honeycomb lattice in the tight binding model for $t = 1/3$.

4.2 Density of states for interacting electrons.

In this section the density of states for interacting electrons will be calculated for the honeycomb lattice. The single-site DMFT method with the iterative perturbation theory, described in the previous chapter is used. The density of states for non-interacting electrons is the only quantity in the self-consistent set of equations that depends on the structure of the lattice. The integral for the local interacting Green's function in Eq. (3.20), is calculated numerically for each cycle of the iterative perturbation theory, using the values of DOS for non-interacting electrons plotted in Fig. 4.5. The obtained density of states for different Coulomb interaction strengths are shown in Fig. 4.6, for $\beta D = D/T = 10$, where $D = 3t$ is the half bandwidth.

For $U = 0$ the obtained density of states is somewhat different from the density of states in Fig. 4.5. Some peaks occur on the positions of the van Hove singularities in the density of states shown Fig. 4.5. The DOS at $\epsilon = 0$ is now finite. This features are present because of the Padé approximation used to convert the Matsubara Green's function to the real time Green's functions.

When the Coulomb interaction is increased, the upper and lower bands are pushed together. For $U = D$ the DOS corresponds to the DOS of a metal. At a value of $U = 2.5D$ the typical tree-peak structure arises with two Hubbard peaks and a quasiparticle peak at $\omega = 0$. When the Coulomb interaction strength is increased further, the coherent peak at the Fermi energy disappears due to the mass enhancement of the quasiparticles. The system undergoes a transition into an insulating state at a critical value of $U_c = 3.1D = 9.3t$.

In Ref. [16], single-site DMFT was also used to study the Mott transition for the honeycomb lattice and a critical transition value of $U_c = 13.3t$ was obtained. In Ref. [18] the semimetal-insulator transition was studied using the Gutzwiller method giving $U_c = 12.8t$. Our calculated value is somewhat smaller then these. The value is, however, very large and well beyond the interaction parameters in graphene for instance.

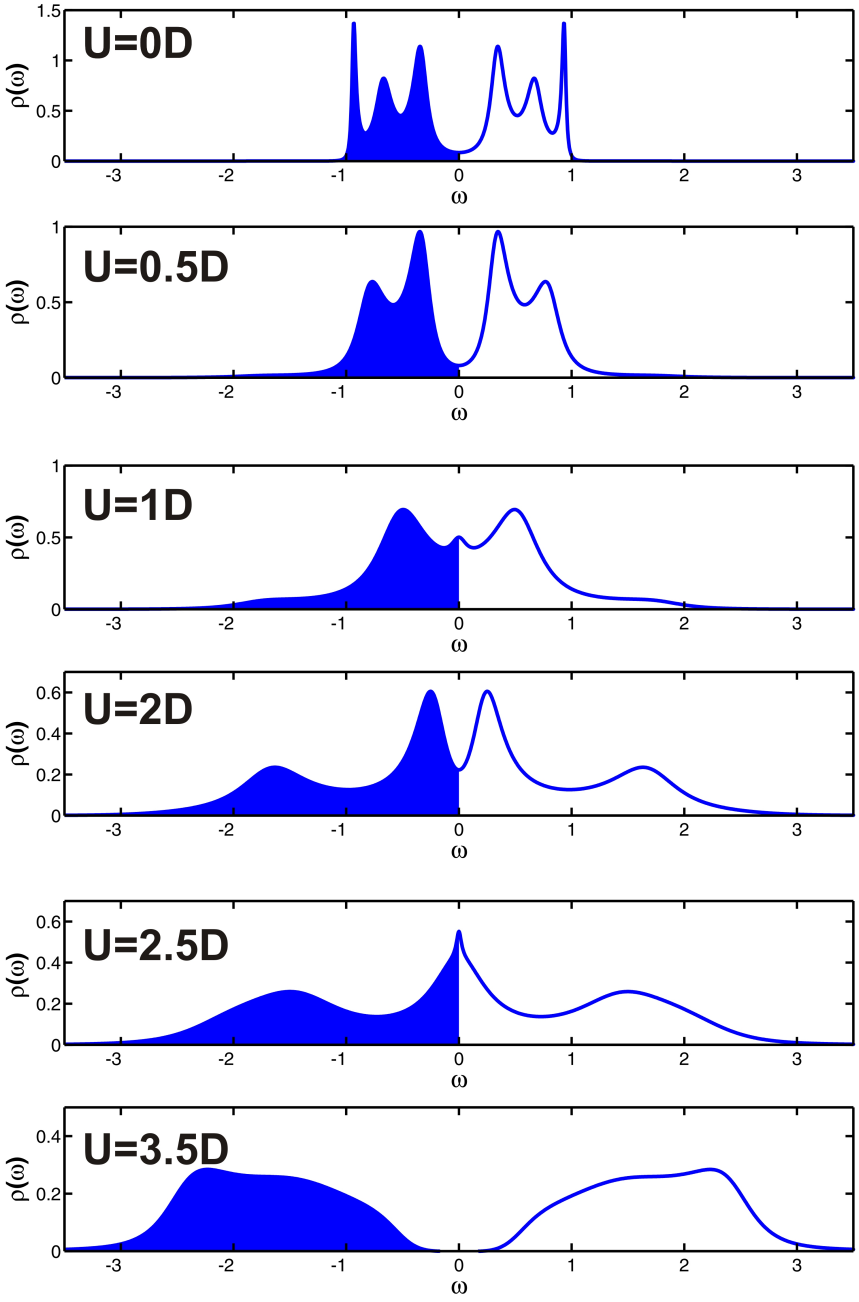

Figure 4.6: The density of states obtained using single-site DMFT for the honeycomb lattice for $U/D = 0, 0.5, 1, 2, 2.5, 3.5$ and $\beta D = 10$.

4.3 Discussion and Conclusion

The results in Fig. 4.6 show that a semimetal-insulator transition is expected to occur at $U_c = 9.3t$. The structure of the transition is very similar to the metal-insulator transition studied in Sec. 3.3. Because the density of states around the Fermi level is small, one would expect that electron-electron scattering gives rise to different effects then for a metallic system. The Dirac fermions on the honeycomb lattice are massless which actually makes the Fermi liquid theory an invalid approach.

The single site DMFT is valid in the limit of large lattice coordination, where non local electron correlations can be neglected. In a low dimensional system like the one dimensional chain, single site DMFT fails [11], because the $\mathbf{k}$ dependence of the self-energy cannot be neglected. The one dimensional chain actually has a perfect nesting instability at half-filling, which can not be described by DMFT, because the Fermi surface does not change when the Coulomb interaction is increased. The honeycomb lattice is a bipartite lattice and also has perfect-nesting instability at half-filling, which can lead to an antiferromagnetic insulating state shown in Fig. 4.7. The honeycomb lattice has a lattice coordination $z = 3$ which is not much larger then the one dimensional chain ($z = 2$). Therefore, the $\mathbf{k}$-dependence of the self-energy for the honeycomb lattice might not be negligible.

Instead of considering a single site in an effective medium, a cluster of sites has to be considered to include non-local electron correlations. Cluster approaches of DMFT exist, and have been used to study the Mott transition on the honeycomb lattice [27]. In the next chapter we will study a different cluster approach, called Cluster Perturbation Theory. We will study the one dimensional chain to see if the method can describe electron correlations properly. Then we will turn to the honeycomb lattice.

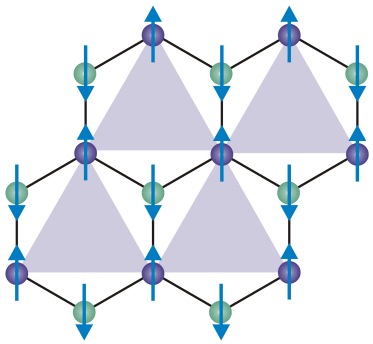

Figure 4.7: The honeycomb lattice at half filling in an insulating antiferromagnetic ground state.

Chapter 5

Cluster Perturbation Theory

In the previous chapter, dynamical mean field theory was used to study the semimetal-insulator transition on the honeycomb lattice. Since a single site in an effective medium was treated, only local electron correlations (on the site) where taken into account. This is valid in the limit of infinite dimensions ($z \to \infty$), where the self-energy is independent of $\mathbf{k}$. The honeycomb lattice however, only has one nearest neighbor more ($z = 3$) than a one-dimensional chain ($z = 2$) for which DMFT fails. Therefore, non-local electron correlations can be important for the honeycomb lattice. Instead of studying a single site in an effective medium, a cluster of sites should be studied.

In this chapter Cluster Perturbation Theory (CPT) introduced by D. Sénéchal *et al.* [17,18] is studied. In CPT the lattice is divided into a superlattice consisting of identical clusters. Exact diagonalization is used to solve the Hubbard model on a cluster. The hopping of electrons between adjacent clusters is treated perturbatively.

Cluster Perturbation Theory is a zero temperature calculation of the probability that an electron has energy ω and wavevector $\mathbf{k}$ called the spectral weight, which can be used to study the Mott transition. The spectral weight can be measured by angle-resolved photoemission spectroscopy and can be compared to the results obtained by CPT.

In Sec. 5.1 we will explain how a lattice can be divided into a superlattice of identical clusters. Then we will discuss the Lanczos method of exact diagonalization, to solve the Hubbard model on a single cluster. The Lanczos method is a numerical technique, and the text is written in such a way that the reader learns how to write an efficient routine. In Sec. 5.2 we explain the strong coupling perturbation theory, used to describe the hopping of electrons

between adjacent clusters. In Sec. 5.3 we apply cluster perturbation theory to a one-dimensional chain. Results for the spectral weight and density of states for the chain will be presented. In Sec. 5.4 we turn to the honeycomb lattice. The CPT is applied, and the semimetal-insulator transition is studied from the spectral weight and density of states.

5.1 Exact Diagonalization

The cluster perturbation starts by dividing a lattice into a superlattice consisting of identical clusters. The clusters are restricted to rather small sizes, e.g. 16 sites for Hubbard systems, because of memory requirements. In Fig. 5.1a, a square lattice is divided into identical four-site square clusters. The sites within a cluster are labeled by $i = 1, ..., 4$. The superclattice is shown at the righthand side and is a square lattice for this choice of clusters. It is important that different shapes and sizes of clusters are studied for a certain lattice to distinguish between the real spectral weight and possible cluster artifacts. In Fig. 5.1b the square lattice for instance, is divided into clusters containing five sites. The lattice sites of the superlattice, which represent the clusters, can be labeled by the vector $\mathbf{R}$.
As stated above, in CPT the Hubbard model is solved by exact diagonalization for an individual cluster, and the intercluster hopping is treated perturbatively. In this section the exact diagonalization for a single cluster will be explained. The goal is to obtain the retarded cluster Green's function, defined as

$$G_{ij}(\omega) =< \phi_0|c_i \frac{1}{\omega - H + E_0} c_j^\dagger|\phi_0 > + < \phi_0|c_i \frac{1}{\omega + H - E_0} c_j^\dagger|\phi_0 >, \qquad (5.1)$$

where ϕ_0 is the ground state of the cluster with energy E_0. The first (second) term describes the propagation of an added electron (hole) from the site i to the site j within the cluster. To calculate these averages, we first need to obtain the ground state of the system. This can be done by calculating the lowest eigenvalue and eigenvector of the Hamiltonian matrix.

We consider the Hubbard model, in which electrons can hop to neighboring sites within the cluster and there is an on-site Coulomb interaction if a site is doubly occupied. The Hubbard Hamiltonian for a single cluster $\mathbf{R}$ can be written as

$$H^0_{\mathbf{R}}(c^\dagger_{\mathbf{R}i\sigma}, c_{\mathbf{R}i\sigma}) \quad = \quad -t \sum_{<ij>\sigma} (c^\dagger_{\mathbf{R}i\sigma} c_{\mathbf{R}j\sigma} + c^\dagger_{\mathbf{R}j\sigma} c_{\mathbf{R}i\sigma}) + \sum_i U n_{\mathbf{R}i\uparrow} n_{\mathbf{R}i\downarrow} \qquad (5.2)$$

where the sum is over all nearest neighbors $< ij >$ within the cluster. The maximum number of electrons on a single site is two and, therefore, each site has four possible states. A cluster consisting of $L = 8$ sites therefore has $4^8 = 65536$ different states. These states together form a basis for the Hamiltonian matrix which has 65536^2 elements. Although a lot of the elements are equal to zero, the matrix is very large and requires substantial memory to store. For cluster

sizes $L > 9$ conventional routines for finding the eigenvalues and eigenvectors do not work anymore because the memory requirements exceed what a computer can handle. The matrix can, of course, be stored on a hard disk, but this makes the routines rather slow.

Cluster perturbation theory is a zero temperature calculation and therefore, we are only interested in the ground state of our system. We thus, need to calculate only the lowest eigenvalue and corresponding eigenvector of the Hamiltonian matrix. There is a method called Lanczos exact diagonalization which can find the extreme (smallest/largest) eigenvalues and eigenvectors of a large matrix without storing the matrix. The method needs a routine, however, that multiplies a vector with the large matrix. This routine produces non-zero elements of the large matrix when needed, but does not store them.

In this section we will explain how the Lanczos method for exact diagonalization works [29]. First we explain how a convenient basis can be created for the Hamiltonian matrix. Then the routine for the multiplying a vector with the Hamiltonian matrix without having to store the matrix is explained. This routine will then be used to derive The Lanczos algorithm for finding the extreme

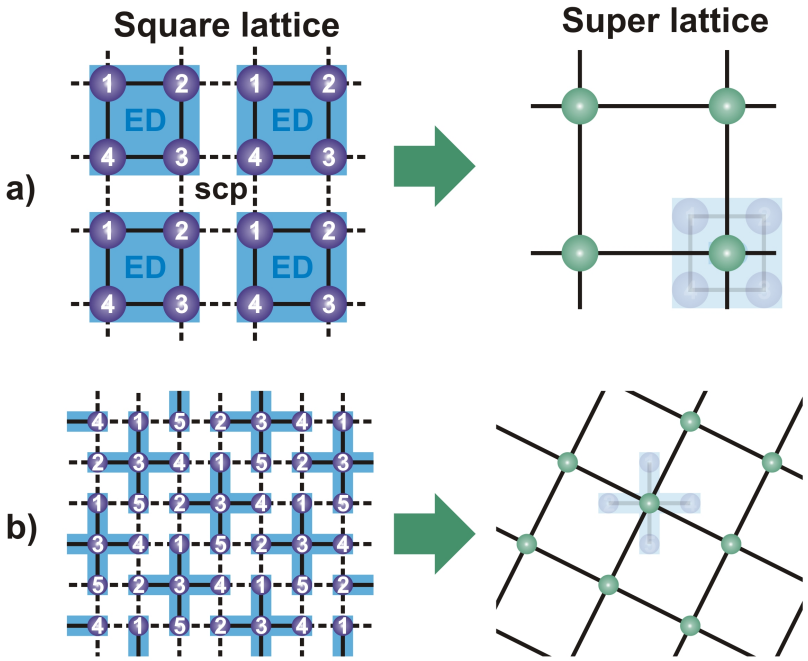

Figure 5.1: (a) The square lattice divided into squared identical clusters of four sites. (b) Exact diagonalization is used within a cluster and intercluster bonds are treated perturbatively.

eigenvalues and eigenvectors. Then we will show that the Lanczos method can actually be used to calculate the averages in Eq. (5.1).

5.1.1 Definition of states

The Hubbard model conserves the electron number and the total spin of electrons. Therefore, the total number of spin-up and spin-down electrons on the cluster is fixed. These symmetries of the Hamiltonian can be used to block-diagonalize the Hamiltonian matrix

$$H = \begin{pmatrix} \begin{pmatrix} \cdot & \cdot \\ \cdot & \cdot \end{pmatrix} & & \mathbf{0} \\ & \begin{pmatrix} \cdot & \cdot & \cdot \\ \cdot & \cdot & \cdot \\ \cdot & \cdot & \cdot \end{pmatrix} & \\ \mathbf{0} & & \begin{pmatrix} \cdot & \cdot & \cdot \\ \cdot & \cdot & \cdot \\ \cdot & \cdot & \cdot \end{pmatrix} \end{pmatrix} \tag{5.3}$$

Each block corresponds to a different number of the spin-up ($N_\uparrow$) and/or spin-down ($N_\downarrow$) electrons. When finding the eigenvalues and eigenvectors of the system the blocks can be treated separately. Other symmetries like the translational invariance of the cluster can be used to create even smaller blocks. In this report, however, only the conservation of particles and spin will be used.

A convenient basis for a single block of the Hamiltonian matrix is the occupation number basis, which consists of all possible states. The sites inside the cluster are labeled by $1, 2.., L$. The configurations of the spin-up and spin-down electrons are treated separately. A "1" is used, if a certain site is occupied by a spin projection σ electron and a "0" if it is unoccupied. An example of a state for a cluster consisting of 6 sites with $N_\downarrow = 2$ and $N_\uparrow = 3$ is

$$|100010>_\downarrow |101001>_\uparrow . \tag{5.4}$$

In this case the spin up electrons are located at the sites labeled by the numbers 1,4 and 6 (right to left). The spin down electrons are located at the sites 2 and 6. The total number of states for a general Hamiltonian block consists of all possible configurations, to place $N_\uparrow$ spin-up electrons and $N_\downarrow$ spin-down electrons over L lattice sites

$$m = \frac{L!}{(L-N_\downarrow)!N_\downarrow!} \times \frac{L!}{(L-N_\uparrow)!N_\uparrow!}. \tag{5.5}$$

Each electron configuration can be described by a binary number of $2L$ bites as in Eq. 5.4. Therefore each state can be uniquely defined by a single integer

corresponding to this binary number

$$\begin{aligned} I &= \sum_{i=1}^{L}(n_{\uparrow}(i)2^{i-1} + n_{\downarrow}(i)2^{(L+i-1)}) \\ &= \sum_{i=1}^{L}(I_{\uparrow} + 2^{L}I_{\downarrow}). \end{aligned} \tag{5.6}$$

Here $n_\sigma(i)$ is the occupation number (0,1) of a site i by a spin projection σ electron. All possible configurations for a cluster consisting of $L = 3$ sites with $N_\uparrow = 2$ and $N_\downarrow = 1$ are shown in the table below. $I_\downarrow$ and $I_\uparrow$ are the integers corresponding to the spin down and spin up configurations respectively.

down configuration	$I_\downarrow$	up configuration	$I_\uparrow$	$I = I_\uparrow + 2^m I_\downarrow$
001	1	011	3	11
001	1	101	5	13
001	1	110	6	14
010	2	011	3	19
010	2	101	5	21
010	2	110	6	22
100	4	011	3	35
100	4	101	5	37
100	4	110	6	38

The 5th column of integers forms a complete basis for the Hamiltonian block. In a program the vector containing all these integers, corresponding to the different states, can be computed easily. It is convenient to calculate first the maximum values that the integers $I_\uparrow$ and $I_\downarrow$ can achieve

$$I_\sigma^{max} = \sum_{i=1}^{N_\sigma} 2^{(m-1-i)}. \tag{5.7}$$

Running a dummy integer from 0 to I_σ^{max} and checking for every step whether the state represents a configuration with N_σ electrons results in an array with all possible I_σ. The two arrays for the spin-up and spin-down states can then be combined, to give all possible integers I which form a basis for the Hamiltonian matrix.

5.1.2 Hamiltonian matrix

The Lanczos method explained in the Sec 5.1.3 will be used to find the lowest eigenvalues and eigenvectors of the Hamiltonian without storing the matrix. The method needs a routine, which, multiplies a vector with the Hamiltonian matrix. The Hamiltonian is a sparse matrix and instead of storing the whole matrix, the goal is to generate the non-zero elements when needed. This can be done efficiently using binary number operations as explained in Ref. [29]. To

show how this is done, a one-dimensional chain of L sites with open boundary conditions is considered as an example. The Hubbard Hamiltonian for the chain is given by Eq. 2.17

$$\mathcal{H}_H = -t \sum_{<i,j>,\sigma} (c^\dagger_{i\sigma} c_{i+1\sigma} + c^\dagger_{i+1\sigma} c_{i\sigma}) + U \sum_i n_{i\sigma} n_{i,-\sigma}. \tag{5.8}$$

It is clear from the first term that hopping can be treated separately for spin-up and spin-down electrons. Because of the Pauli principle hopping between neighboring sites is allowed when their spin-σ occupation is either 01 or 10. The following trick can be used to check the possibility for hopping between the site i and the site $i+1$, for a configuration $I_\uparrow$. First a mask (binary number) is created with non-zero bits at the sites of interest only ($2^{i-1}+2^i$). Then a binary AND operation is performed using the mask and binary representation of $I_\uparrow$. The result is called K. Then an exclusive or (XOR) operation is performed using K and the mask. When the result M of this operation has the configuration 01 or 10 at the sites of interest, the hopping is possible. The state after hopping is then given by $I_\uparrow + M - K$. The element in the Hamiltonian matrix connecting the state before hopping and after hopping is then equal to $-t$. An example of the procedure is shown in the table below, where it is checked if hopping between sites 2 and 3 is possible.

$I_\uparrow$	1010	
mask	0110	AND
K	0010	
mask	0110	XOR
M	0100	
$I^{new}_\uparrow$	1100	

The same procedure can be used for the spin-down electrons. The Coulomb interaction can be checked in a similar way. Coulomb interaction is present at a site i, if it is occupied by a spin-up and a spin-down electron. Therefore a mask is created equal to $2^{i-1}+2^{L+i-1}$. Then an AND operation with the mask and the state I is performed. If the result equals the mask, the site contains two electrons and the Coulomb interaction is present. The diagonal element corresponding to the state is then increased by U. The same check is then done for the next site.

The non-zero elements of the Hamiltonian matrix can be calculated using these techniques. This can be used in the routine where the Hamiltonian matrix is multiplied with a vector: $\mathcal{H}\mathbf{y} = \mathbf{x}$. First the vector $\mathbf{x} = 0$. When a non-zero element of the matrix $\mathcal{H}$ is generated, it is immediately multiplied with the corresponding element of the vector $\mathbf{y}$ and added to the right element of $\mathbf{x}$. The matrix element can then be forgotten, and a new nonzero element is calculated.

In this way the Hamiltonian matrix does not have to be stored. Here the one dimensional chain was studied. Different lattices can be studied using the same

technique. One has to conveniently label the sites within a cluster and create the right mask for the hopping term. The 4 site cluster for the square lattice in Fig. 5.1a is actually a one dimensional chain with periodic boundary conditions. The above, can therefore, be applied to this system.

5.1.3 Lanczos method

The Lanczos method is commonly used to find the smallest and largest eigenvalues, and the corresponding eigenvectors of a large matrix. As already mentioned, the method does not require the matrix to be stored. However, a routine is needed, which multiplies the matrix with a vector. In our case the large matrix is a block of the Hamiltonian matrix corresponding to a fixed number of spin-up and spin-down electrons. The block is denoted by A which is symmetric and has dimension $n \times n$.

A subspace can be defined as the set of all n-vectors that are linear combinations of the set $S = \{\mathbf{s}_1, \mathbf{s}_2 ..., \mathbf{s}_m\}$ containing m vectors. The subspace is invariant under a matrix A, if for each vector $\mathbf{x}$ in the subspace, the product $A\mathbf{x}$ lies within the subspace. The eigenvalues λ of a matrix can be found by solving the equation for the characteristic polynomial

$$|A - \lambda I| = 0. \tag{5.9}$$

Lanczos tried to find this polynomial by generating vectors which form a basis for the invariant subspace of the matrix A. He started with a random vector $\mathbf{q}_0$ with dimension n. The next vector $\mathbf{q}_1$ is chosen as a linear combination of $\mathbf{q}_0$ and $A\mathbf{q}_0$

$$\beta_0 \mathbf{q}_1 = A\mathbf{q}_0 - \alpha_0 \mathbf{q}_0. \tag{5.10}$$

The constant α_0 is chosen such that the inner product $\mathbf{q}_1 \cdot \mathbf{q}_1 = |\mathbf{q}_1|^2$ is minimal:

$$\alpha_0 = \frac{(A\mathbf{q}_0) \cdot \mathbf{q}_0}{|\mathbf{q}_0|^2}. \tag{5.11}$$

For this choice of α_0, the vectors $\mathbf{q}_0$ and $\mathbf{q}_1$ are orthogonal

$$\mathbf{q}_0 \cdot \mathbf{q}_1 = 0. \tag{5.12}$$

The next vector is then chosen again chosen as a linear combination of the previous vectors

$$\beta_1 \mathbf{q}_2 = A\mathbf{q}_1 - \alpha_1 \mathbf{q}_1 - \beta_1 \mathbf{q}_0. \tag{5.13}$$

Again minimizing the squared length of $\mathbf{q}_2$ results in the following expression for the constants:

$$\alpha_1 = \frac{(A\mathbf{q}_1) \cdot \mathbf{q}_1}{|\mathbf{q}_1|^2}, \qquad \beta_1 = \frac{(A\mathbf{q}_1) \cdot \mathbf{q}_0}{|\mathbf{q}_0|^2}. \tag{5.14}$$

The vector $\mathbf{q}_2$ is orthogonal to both $\mathbf{q}_0$ and $\mathbf{q}_1$. The third vector is in complete analogy defined as

$$\beta_2 \mathbf{q}_3 = A\mathbf{q}_2 - \alpha_2 \mathbf{q}_2 - \beta_2 \mathbf{q}_1 - \gamma_0 \mathbf{q}_0. \tag{5.15}$$

If the inner product $\mathbf{q}_3 \cdot \mathbf{q}_3$ is minimized, one finds that due to the orthogonality of $\mathbf{q}_0$, $\mathbf{q}_1$ and $\mathbf{q}_2$,

$$\begin{aligned} \alpha_2 &= \frac{(A\mathbf{q}_2)\mathbf{q}_2}{|\mathbf{q}_2|^2}, \qquad \beta_2 = \frac{(A\mathbf{q}_2)\mathbf{q}_1}{|\mathbf{q}_1|^2} \\ \gamma_0 &= \frac{(A\mathbf{q}_2)\mathbf{q}_0}{\mathbf{q}_0^2} - \frac{\beta_1 \mathbf{q}_1 \mathbf{q}_0}{\mathbf{q}_0^2} = 0. \end{aligned} \tag{5.16}$$

Since $\gamma_0 = 0$, the new vector can be calculated using the previous two vectors only. This can be shown for every vector. The recursion relation for a new vector is given by

$$\beta_j \mathbf{q}_{j+1} = A\mathbf{q}_j - \alpha_j \mathbf{q}_j - \beta_{j-1} \mathbf{q}_{j-1}. \tag{5.17}$$

The new vector is orthogonal to the previous vectors. The set of vectors $K = \{\mathbf{q}_0, \mathbf{q}_1, ..., \mathbf{q}_m\}$ generated in this way, clearly forms a basis for an invariant subspace of the matrix A. The subspace K is called a Krylov space.

The matrix $Q = (\mathbf{q}_0, \mathbf{q}_1, ..., \mathbf{q}_m)$ $(n \times m)$ is defined as the matrix containing m generated basis vectors in its columns. The basis vectors in the matrix Q are orthogonal and can be normalized so that $Q^T Q = I$. Since the subspace K is invariant, the product $A\mathbf{q}_i$ lies within the subspace and can be written as a linear combination of the basis vectors in Q. Therefore

$$AQ = QT, \tag{5.18}$$

where T is a $(m \times m)$ matrix containing the linear combination constants. If the matrix T has an eigenvector $\mathbf{y}$ with eigenvalue λ, then

$$QT\mathbf{y} = \lambda Q\mathbf{y}, \tag{5.19}$$

where both sites of the eigenvector equation are multiplied by the matrix Q. Using Eq. 5.18 this can be rewritten as

$$A(Qy) = \lambda(Qy). \tag{5.20}$$

Any eigenvalue λ of the matrix T is thus an eigenvalue of the larger matrix A. The corresponding eigenvector of A is Qy. The matrix T has the following tridiagonal form

$$T = \begin{pmatrix} \alpha_0 & \beta_0 & & & & \\ \beta_0 & \alpha_1 & \beta_1 & & & \\ & \beta_1 & \alpha_2 & \beta_2 & & \\ & & \cdot & \cdot & \cdot & \\ & & & \beta_{m-2} & \alpha_{m-1} & \beta_{m-1} \\ & & & & \beta_{m-1} & \alpha_m \end{pmatrix}. \tag{5.21}$$

The matrix is symmetric and can be stored by two vectors with m entries.

The Lanczos algorithm works the following way. The method starts by generating a random normalized vector $\mathbf{q}_0$ of dimension n. Using the recurrence relation in Eq. 5.17 new vectors are generated. The coefficients α_j and β_j are calculated, and stored in vectors $\boldsymbol{\alpha}$ and $\boldsymbol{\beta}$. Because of the recurrence relation (Eq. 5.17), only the last two generated $\mathbf{q}$ vectors have to be stored. The generating of new vectors stops when a coefficient $\beta_j = 0$ or when 400 vectors have been generated. The convergence of the Lanczos algorithm is fast for extreme eigenvalues and generating 400 vectors is usually enough even for 16 million by 16 million matrices [29]. The eigenvalues and eigenvectors of the matrix T are then found using a conventional routine for a tridiagonal matrix. The lowest eigenvalue found, is the lowest eigenvalue of the large matrix A. The corresponding eigenvector of A is $\boldsymbol{\phi} = Q\mathbf{y}$. The matrix Q however has not been stored, since it is very large and only the last two vectors are needed to create a new orthonormal vector. Therefore, after finding the eigenvector $\mathbf{y}$ of T the Lanczos algorithm has to be restarted using the same random initial vector $\mathbf{q}_0$. The generated $\mathbf{q}_i$ vectors are immediately used for the multiplication $Q\mathbf{y}$ and, therefore, do not have to be stored. The eigenvector of A is stored during the routine in a third vector.

The extreme eigenvalues and eigenvectors of a large $n \times n$ matrix can thus be found by finding the eigenvalues and eigenvalues of a much smaller tridiagonal $m \times m$ matrix. The algorithm needs a routine that can perform the multiplication $A\mathbf{q}_i$ however. Only three vectors of dimension n and two vectors of dimension m have to be stored.

5.1.4 Cluster Green's function

At zero temperature the system will be in the ground state. It has an energy E_0 equal to the lowest eigenvalue of the Hamiltonian block A. The corresponding eigenvector ϕ_0 describes the state and can be obtained using the Lanczos algorithm, as described above. Since the number of electrons in the cluster is fixed, we can write $A = H$. The retarded real time cluster Green's function is a matrix in site indices i, j:

$$G_{ij\sigma}(\omega) = \sum_{\sigma} \left(G^e_{ij}(\omega) + G^h_{ij}(\omega) \right), \tag{5.22}$$

where the first part corresponds to the propagation of an electron and the second part to the propagation of a hole

$$G^e_{ij\sigma}(\omega) = < \phi_0 | c_{i\sigma} \frac{1}{\omega - H + E_0} c^\dagger_{j\sigma} | \phi_0 > \tag{5.23}$$

$$G^h_{ij\sigma}(\omega) = < \phi_0 | c^\dagger_{i\sigma} \frac{1}{\omega + H - E_0} c_{j\sigma} | \phi_0 > . \tag{5.24}$$

Here H is the Hamiltonian which is a large matrix. The Lanczos algorithm can be used to tridiagonalize H and to obtain the cluster Green's function. The average

$$< \phi_0 | C \frac{1}{\omega - H + E_0} C^\dagger | \phi_0 >, \tag{5.25}$$

where C is an operator containing creation/annihilation operators with hermitian conjugate $C^\dagger$ can be calculated in the the following way. First $C|\phi_0>$ is calculated and used as the initial vector in the Lanzos algorithm. The coefficients α_i and β_i are calculated as described in the previous section. The average in Eq. 5.25 is then equal to the following continued fraction [25],

$$\frac{1}{\omega + E_0 - \alpha_1 - \frac{\beta_1^2}{\omega + E_0 - \alpha_2 - \frac{\beta_2^2}{\ddots}}}. \tag{5.26}$$

By choosing $C = c_{i\sigma}$ the diagonal element $G^e_{ii}(\omega)$ is calculated. Off-diagonal elements cannot be calculated directly using the continued fraction, since $(c_{i\sigma})^\dagger \neq c^\dagger_{j\sigma}$. The four averages with $C = c_{i\sigma} \pm c_{j\sigma}$ and $C = c_{i\sigma} \pm i c_{j\sigma}$ can, however, be calculated using the continued fraction. An off-diagonal term of the retarded Green's function is then given by

$$\begin{aligned} < \phi_0 | c_{i\sigma} \frac{1}{\omega - H + E_0} c^\dagger_j | \phi_0 > \quad = \quad & \frac{1}{4} \Big[< | (c_{i\sigma} + c_{j\sigma}) \frac{1}{\omega - H + E_0} (c^\dagger_i + c^\dagger_j) | > \\ & - < | (c_{i\sigma} - c_{j\sigma}) \frac{1}{\omega - H + E_0} (c^\dagger_i - c^\dagger_j) | > \\ & + i < | (c_{i\sigma} + i c_{j\sigma}) \frac{1}{\omega - H + E_0} (c^\dagger_i - i c^\dagger_j) | > \\ & - i < | (c_{i\sigma} - i c_{j\sigma}) \frac{1}{\omega - H + E_0} (c^\dagger_i + i c^\dagger_j) | > \Big] \end{aligned} \tag{5.27}$$

For the hole part of the cluster Green's function the same technique can be used. For this the creation and annihilation operators have to be interchanged and the Hamiltonian matrix as well as E_0 get an additional minus sign. The Green's function $G_{ij}(\omega)$, can be directly used for the calculation of the spectral weight for the small cluster, which for instance is done in Ref. [30][31]. The method of exact diagonalization is, however, confined to small cluster sizes (16 sites). Therefore, we have to include the intercluster hopping, which is described in the next section.

5.2 Strong coupling perturbation theory

In the calculation of the cluster Green's function described in the previous section, electrons where only allowed to hop to neighboring sites within the cluster and, therefore, the total number of electrons on the cluster was conserved. Now

the intercluster hopping is taken into account using the strong-coupling perturbation theory (SCPT), which is described in references [20-23,26]. Here we give a summary of the derivation in reference [21].

The Hubbard Hamiltonian for a lattice divided into identical clusters can be written as

$$\mathcal{H} = \sum_{\mathbf{R}} H^0_{\mathbf{R}}(c^\dagger_{\mathbf{R}i\sigma}, c_{\mathbf{R}i\sigma}) + \sum_{\mathbf{R}\mathbf{R}'ij\sigma} V_{ij}^{\mathbf{R}\mathbf{R}'} c^\dagger_{i\mathbf{R}\sigma} c_{i\mathbf{R}\sigma}, \tag{5.28}$$

where $H^0_{\mathbf{R}}$ is the Hamiltonian on a single cluster defined in Eq. (5.2), and $V_{ij}^{\mathbf{R}\mathbf{R}i'}$ is the hopping amplitude between the sites i and j located in adjacent clusters $\mathbf{R}$ and $\mathbf{R}'$ respectively. In SCPT the hopping of electrons is treated perturbatively and the Coulomb interaction term is dominant. Using Grassmann variables $\gamma_{\mathbf{R}i\sigma}$ corresponding to the operator $c_{\mathbf{R}i\sigma}$, the partition function for the Hubbard Hamiltonian at a temperature $\beta = 1/T$ can be written as

$$Z = \int D\gamma^\dagger_{\mathbf{R}i\sigma} D\gamma_{\mathbf{R}i\sigma} e^{-S_H(\gamma^\dagger_{\mathbf{R}i\sigma}, \gamma_{\mathbf{R}i\sigma})}, \tag{5.29}$$

where the action for the Hubbard model is given by Eq. (3.23), which can be written as

$$\begin{aligned} S_H = \int_0^\beta d\tau \Big[\sum_{\mathbf{R}i\sigma} \gamma^\dagger_{\mathbf{R}i\sigma}(\tau)(\frac{\partial}{\partial\tau} - \mu)\gamma_{\mathbf{R}i\sigma}(\tau) + \sum_{\mathbf{R}} H^0_{\mathbf{R}}(\gamma^\dagger_{\mathbf{R}i\sigma}, \gamma_{\mathbf{R}i\sigma}) \\ + \sum_{\mathbf{R}\mathbf{R}',ij} V_{ij}^{\mathbf{R}\mathbf{R}'} \gamma^\dagger_{\mathbf{R}i\sigma}(\tau)\gamma_{\mathbf{R}'j\sigma}(\tau) \Big]. \end{aligned} \tag{5.30}$$

The last term describes the hopping of electrons and is treated perturbatively. The action can be written in a more convenient way making use of the bra-ket notation. The last term for example can be written as

$$\int_0^\beta d\tau \sum_{\mathbf{R}\mathbf{R}'ij\sigma} V_{ij}^{\mathbf{R}\mathbf{R}'} \gamma^\dagger_{\mathbf{R}i\sigma}(\tau)\gamma_{\mathbf{R}'j\sigma}(\tau) = \sum_{\mu\nu} V_{\mu\nu}\gamma^\dagger_\mu\gamma_\nu = <\gamma|\hat{V}|\gamma>, \tag{5.31}$$

where μ and ν denote sets of indices $(i, \mathbf{R}, \sigma, \tau)$, and $\hat{V}$ is the hopping matrix $V_{ab}^{\mathbf{R}\mathbf{R}'}$. The non-perturbative part of the Hamiltonian (Coulomb term) is quartic in creation and annihilation operators. Wick theorem only applies to non-perturbative quadratic Hamiltonians and, therefore, can not be used. This makes it difficult to calculate the self-energy and obtain the diagrammatic rules.

The partition function can be rewritten in a quadratic form in terms of auxiliary Grassmann fields $\phi_{\mathbf{R}i\sigma}$ and $\phi^\dagger_{\mathbf{R}i\sigma}$ using the Grassmannian Hubbard-Stratonovich transformation. The transformation expresses the perturbation part of the partition function as a Gaussian integral over the auxiliary fields

$$e^{-<\gamma|\hat{t}|\gamma>} = Det[V] \int D\phi^\dagger D\phi e^{<\phi|V^{-1}|\phi>+<\phi|\gamma>+<\gamma|\phi>}. \tag{5.32}$$

Using this expression the partition function can be written as

$$Z = Z_0 \int D\phi^\dagger D\phi e^{<\phi|V^{-1}|\phi>} \left\langle e^{<\phi|\gamma>+<\gamma|\phi>} \right\rangle_0, \tag{5.33}$$

where $< ... >_0$ is the average with respect to the unperturbed Hamiltonian over the original field γ. In Ref. [21] it is shown that the average in this equation can be written as

$$\begin{aligned} \left\langle e^{<\phi|\gamma>+<\gamma|\phi>} \right\rangle_0 &= exp\Big[\sum_{R=1}^{\infty} \frac{1}{(R!)^2} \sum_{\mathbf{R}\{a_l,a_l'\}} \int_0^\beta \prod_{l=1}^{R} d\tau_l d\tau_l' \\ &\times \phi^\dagger_{\mathbf{R}a_1}(\tau_1)...\phi^\dagger_{\mathbf{R}a_R}(\tau_R)\phi_{\mathbf{R}a_1'}(\tau_R')...\phi_{\mathbf{R}a_R'}(\tau_1') \\ &\times < \gamma_{\mathbf{R}a_1}(\tau_1)...\gamma_{\mathbf{R}a_R}(\tau_R)\gamma^\dagger_{\mathbf{R}a_R'}(\tau_R')...\gamma^\dagger_{\mathbf{R}a_1'}(\tau_1) >_{0,c} \Big], \end{aligned} \tag{5.34}$$

where $< ... >_0, c$ is the so called cumulant average. Note that the operators all share the same cluster index $\mathbf{R}$. Using this expression, the partition function can be rewritten as

$$Z = Z_0 \int D\phi^\dagger D\phi e^{-S_0(\phi^\dagger,\phi)+\sum_{R=1}^{\infty} S^R_{int}(\phi^\dagger,\phi)}, \tag{5.35}$$

where the free quadratic part of the action is given by

$$S_0(\phi^\dagger,\phi) = - < \phi|\hat{V}|\phi > . \tag{5.36}$$

The free propagator of the auxiliary fermions is thus given by $\hat{V}$. An infinite number of interaction terms contribute to action

$$S^R_{int}(\phi^\dagger,\phi) = \frac{-1}{(R!)^2} \sum_{\{\mu_l,\nu_l\}} \phi_{\mu_1}...\phi_{\mu_R}\phi^\dagger_{\nu_R}...\phi^\dagger_{\nu_1} G^{(R)}_{\nu_1...\nu_R,\mu_1...\mu_R}, \tag{5.37}$$

where

$$G^{(R)}_{\nu_1...\nu_R,\mu_1...\mu_R} =< \gamma_{\nu_1}(\tau_1)...\gamma_{\nu_R}(\tau_R)\gamma^\dagger_{\nu_R}(\tau_R')...\gamma^\dagger_{\nu_1}(\tau_1') >_{0,c}, \tag{5.38}$$

is the Green's function on a cluster in terms of the original electron operators. The sum in Eq. (5.37) is over all μ_l, ν_l with the same cluster index $\mathbf{R}$. The partition function in terms of the auxiliary field has the quadratic form, to which Wick theorem can be applied. The interaction term can be treated perturbatively and the self-energy can be calculated.

For the cluster perturbation theory we will only include the $R = 1$ interaction term. The expression in Eq. 5.37 then reduces to

$$S^1_{int}(\phi^\dagger,\phi) = -\sum_{\mu\nu} \phi_\mu \phi^\dagger_\nu G^1_{\mu\nu} =< \phi|\hat{G}|\phi >, \tag{5.39}$$

where $\hat{G}$ is the matrix $\delta_{\mathbf{RR}'}G_{ij}$, and is exactly the cluster Green's function (Eq. (5.22)) calculated in the previous section. It is clear that for $R = 1$, the self-energy of the auxiliary Green's function is equal to the exact electron Green's function on the cluster ($\hat{\Sigma} = \hat{G}$). The connection between the two-point electron Green's function $\mathcal{G}_{ab} =< \gamma_a \gamma_b^\dagger >$ and the free propagator of the auxiliary Grassmann field is given by the Dyson equation

$$\hat{\mathcal{G}} = \frac{1}{\hat{\Sigma}^{-1} - \hat{V}}. \tag{5.40}$$

Using $\hat{\Sigma} = \hat{G}$ this can be rewritten as

$$\hat{\mathcal{G}}(\omega) = \hat{G}(\omega)\frac{1}{1 - \hat{V}\hat{G}(\omega)}. \tag{5.41}$$

The matrices $\hat{G}$ and $\hat{V}$ are invariant under translation with a lattice vector of the superlattice. The Fourier transform of the hopping matrix and Green's function for the superlattice is

$$V_{ij}(\mathbf{Q}) = \frac{1}{N}\sum_{\mathbf{R}} V_{ij}^{0\mathbf{R}} e^{i\mathbf{Q}\cdot\mathbf{R}} \tag{5.42}$$

$$G_{ij}(\mathbf{Q},\omega) = \frac{1}{N}\sum_{\mathbf{R}} G_{ij}^{0\mathbf{R}}(\omega) e^{i\mathbf{Q}\cdot\mathbf{R}} \tag{5.43}$$

Here $\mathbf{Q}$ is a wavevector of the reciprocal lattice of the superlattice. A certain cluster has been chosen as the origin and is labeled by 0. Eq. 5.41 can then be written as

$$\mathcal{G}_{ij}(\mathbf{Q},\omega) = \Big(\hat{G}(\omega)\frac{1}{(1 - \hat{V}(\mathbf{Q})\hat{G}(\omega))}\Big)_{ij} \tag{5.44}$$

The single electron Green's function of the lattice is thus expressed as a combination of the hopping matrix between adjacent clusters, and the cluster Green's function which can be obtained by the exact diagonalization as was explained in the previous section. The electron Green's function of the lattice is in a mixed representation since the cluster Green's function is defined in real space and the hopping matrix in the reciprocal lattice space of the superlattice. In the next section we will use this expression, to calculate the spectral weight and density of states for a one-dimensional chain to illustrate the method.

5.3 One dimensional chain

Here the cluster perturbation theory will be used to calculate the spectral weight and the density of states of a one-dimensional chain. In Fig. 5.2 the one-dimensional chain is shown twice, divided into identical clusters with $L = 2$ (a) and $L = 4$ (b) sites. The cluster Green's function $G_{ij}(\omega)$ can be obtained for

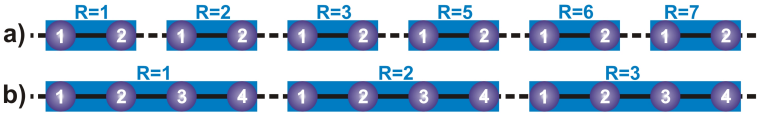

Figure 5.2: The one dimensional chain divided into clusters containing $L = 2$ (top) and $L = 4$ (bottom) sites.

both cluster sizes using exact diagonalization described in Sec. 5.1. It is clear from Fig. 5.2 that intercluster hopping is only possible at the $i = 1$ and $i = L$ site of the clusters. The intercluster matrix is thus given by

$$V_{ij}^{RR'} = -t(\delta_{R,R'-1}\delta_{i,L}\delta_{j,1} + \delta_{R,R'+1}\delta_{i,1}\delta_{j,L}). \tag{5.45}$$

Calculating the Fourier transform of this expression (see Eq. (5.43)), we obtain

$$V_{ij}(Q) = -t(e^{iQ}\delta_{i,L}\delta_{j,1} + e^{-iQ}\delta_{i,1}\delta_{j,L}) \tag{5.46}$$

The electron Green's function matrix $\hat{\mathcal{G}}(Q, \omega)$ can then be obtained using Eq. (5.44). This expression is defined in the reciprocal space of the superlattice and real space within a cluster. We need an expression for the function in the reciprocal space of the lattice. The translational symmetry within a cluster is broken since the bonds between sites within the cluster are treated differently than the bonds between sites located in different clusters. The translational symmetry of the superlattice is, however, still conserved. Due to this the Green's function $\mathcal{G}$ depends on two wave vectors k and k'. The difference between the wave vectors $k - k'$ equals a reciprocal vector of the superlattice, because of the translational invariance.

The one dimensional-chain is divided into N clusters containing L sites. The reciprocal lattice of a one-dimensional chain with lattice constant a is a one dimensional-chain with lattice spacing $\frac{2\pi}{a}$. In the reduced Brillion zone the wavevector k has the values,

$$k = \frac{2\pi n_i}{NLa}, \qquad n_i = 0, 1, 2, ..., NL - 1. \tag{5.47}$$

The superlattice of the one-dimensional chain has a lattice spacing La. Therefore, the reciprocal superlattice has a lattice spacing $\frac{2\pi}{La}$, which is smaller than the reciprocal lattice vector of the real chain. In the reduced Brillion zone the values of the wavevector Q are

$$Q = \frac{2\pi n_j}{NLa}, \qquad n_j = 0, 1, 2, ..., N - 1. \tag{5.48}$$

The Fourier transform of the creation/annihilation operator for an electron located in the cluster R, at intercluster site r_i is given by

$$c_{Ri\sigma} = \frac{1}{\sqrt{LN}} \sum_k c_{k\sigma} e^{ik\cdot(R+r_i)} \tag{5.49}$$

$$c^\dagger_{Ri\sigma} = \frac{1}{\sqrt{LN}} \sum_k c_{k\sigma} e^{-ik\cdot(R+r_i)}, \tag{5.50}$$

The single-electron Green's function in terms of the wave vectors k and k' can then be written as

$$\mathcal{G}(k,k',\omega) = \frac{1}{NL} \sum_{RR'ij} \mathcal{G}^{RR'}_{ij}(\omega) e^{-ik(R+r_i)} e^{ik'(R'+r_j)}. \tag{5.51}$$

Using Eq. (5.43) this can be rewritten as

$$\mathcal{G}(k,k',\omega) = \frac{1}{NL} \sum_{RR'Qij} \mathcal{G}_{ij}(Q,\omega) e^{-ik(R+r_i)} e^{ik'(R'+r_j)} e^{iQ(R-R')}. \tag{5.52}$$

In Fig. 5.3 the reciprocal lattice is shown for the one-dimensional chain and the superlattice. It is clear from the figure that a wavevector k belonging to the reduced Brillion zone of the chain can be decomposed as $k = K + \widetilde{k}$, where K belongs to the reduced Brillion zone of the reciprocal lattice of the superlattice, and $\widetilde{k}$ is a reciprocal lattice vector of the superlattice. The expression

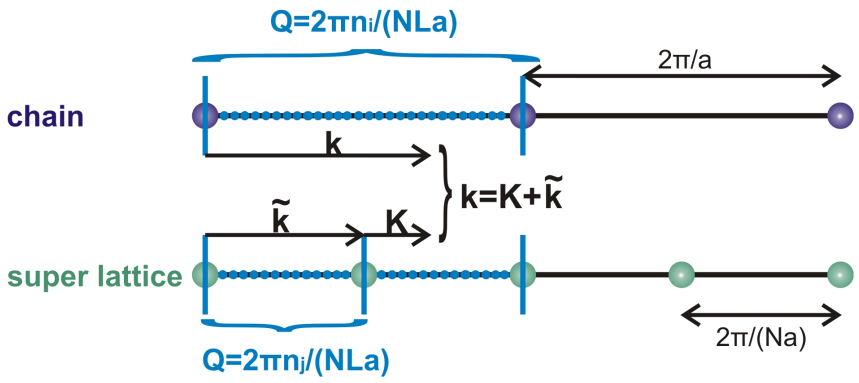

Figure 5.3: The reciprocal lattice for the one-dimensional chain (purple) and superlattice (green) for $L = 2$ is shown. The reduced Brillion zone is in between the blue vertical lines. The wavevector k, in the reduced Brillion zone of the one-dimensional chain can be decomposed in a reciprocal lattice vector $\widetilde{k}$ of the superlattice and a vector K belonging to the reduced Brillion zone of the super lattice $k = \widetilde{k} + K$.

for the electron Green's function in Eq. (5.44), is invariant, if the wavevector

Q is translated by a reciprocal lattice vector of the superlattice. Therefore, $\mathcal{G}_{ij}(k,\omega) = \mathcal{G}_{ij}(Q-\widetilde{k},\omega) = \mathcal{G}_{ij}(K,\omega)$. Performing the summation in Eq. 5.52 we get,

$$\mathcal{G}(\mathbf{k},\mathbf{k}',\omega) = \frac{1}{L}\sum_{ij}\mathcal{G}_{ij}e^{-i\mathbf{k}\mathbf{r}_i}e^{i\mathbf{k}'\mathbf{r}_j}\delta(\mathbf{K}-\mathbf{K}'), \tag{5.53}$$

where

$$\delta(K-K') = \sum_{s=0}^{L-1}\delta(k-k'+\frac{2\pi s}{Na}). \tag{5.54}$$

In the limit of an infinite lattice $N\to\infty$, only the $s=0$ term is important. Performing the sum over k', then reduces the expression for the Green's function to

$$\mathcal{G}_{cpt}(k,k',\omega) = \frac{1}{L}\sum_{i,j=1}^{L}\mathcal{G}_{ij}(k,\omega)e^{ik(r_j-r_i)}. \tag{5.55}$$

The electron Green's function in the reciprocal space of the lattice can thus be obtained by using this equation. The probability that an electron with a wavevector k has a frequency ω (spectral weight) is then

$$A(k,\omega) = -2Im[\mathcal{G}_{cpt}(k,\omega+i\eta+\mu)] \tag{5.56}$$

where $i\eta$ is a small imaginary number added to give a finite width to the poles of the Green's function and μ is the chemical potential. The density of states can be found by summing the spectral weight over all wave vectors within the first Brillion zone

$$\rho(\omega) = \sum_{k\in B.Z.}A(\mathbf{k},\omega+i\eta+\mu). \tag{5.57}$$

5.3.1 Results

In Fig. 5.4 the spectral weight is shown for the one-dimensional chain at half filling with $L=2$ corresponding to Fig. 5.2a), for $U=0$ and $U=4t$ and different values of the wavevector k. The parameters used for this calculation are $N=2000$ and $\eta=0.01$. The exact diagonalization on the cluster is done for $N_\uparrow = N_\downarrow = 1$. For $U=0$ the expected spectral weight is obtained. The $k=\pi/2$ gives a finite contribution to the spectral weight at $\omega=0$. The spectral weight, however, disappears at $\omega=0$ when the Coulomb interaction is increased. For $U=4t$ a clear Hubbard gap (separation $U/2$) is seen at $k=\pi/2$ corresponding to an insulating state. Cluster perturbation theory is exact in the limit of infinite cluster sizes $L\to\infty$. It is thus better to treat larger clusters. The density of states for the one dimensional chain divided into clusters with $L=4$ is shown in Fig. 5.5. For $U=0$ the figure corresponds to the density of states shown in

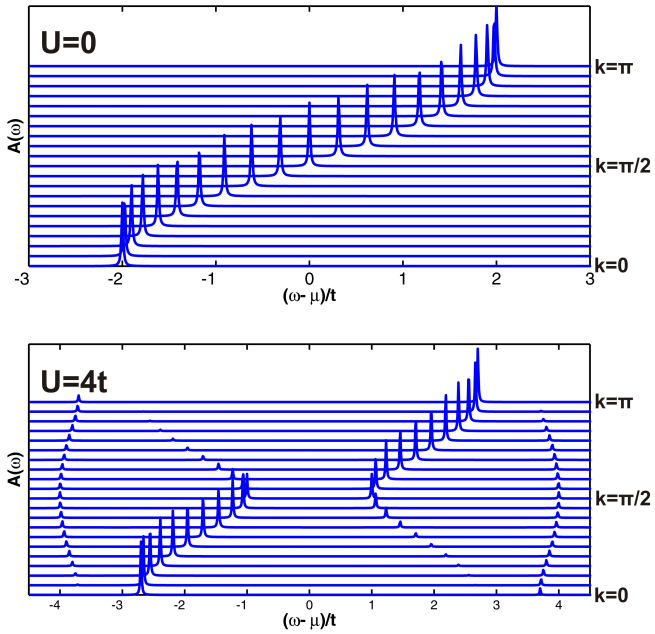

Figure 5.4: Spectral weight for the one-dimensional chain with $L = 2$ for $k = 0, \frac{\pi}{20}, \frac{2\pi}{20}, ..., \pi$ for $U = 0$ (top) and $U = 4t$ (bottom). The values for the parameters are: $t = 1$ and $\eta = 0.01$. The number of clusters considered are $N = 2000$.

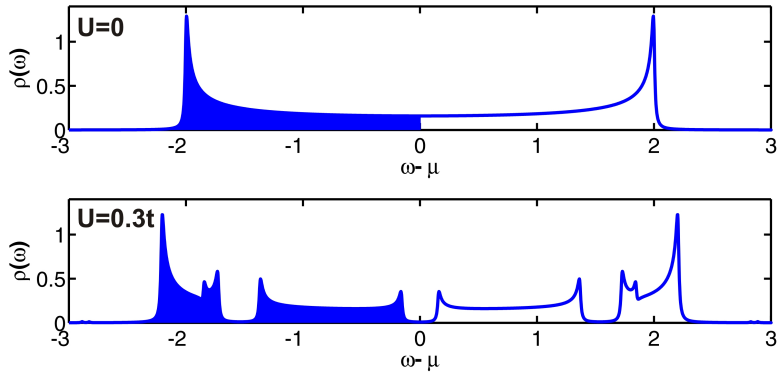

Figure 5.5: DOS for the one-dimensional chain with $L = 4$ for $U = 0$ (top) and $U = 0.3t$ (bottom). The values for the parameters used are $t = 1$, $\eta = 0.01$ and $N = 2000$.

Fig. 3.2 for the hypercubic lattice with $d = 1$. For a small value of $U = 0.3t$, a gap already appears at the Fermi energy and the chain is in an insulating state. The cluster perturbation theory takes into account local electron correlations (k-dependence of the self-energy) on the cluster and can describe the insulating one-dimensional chain properly.

The cluster perturbation theory is exact when there is no Coulomb interaction. The Hamiltonian in Eq. (5.28) when $U = 0$, becomes quadratic in creation/annihilation operators and the Wick theorem applies. If the intercluster hopping is treated perturbatively to hopping within a cluster, the self-energy is exactly $\widehat{V}$ and, therefore,

$$\widehat{\mathcal{G}} = \frac{1}{\widehat{G}^{-1} - \widehat{V}}. \tag{5.58}$$

This formula is the same as for the cluster perturbation theory in Eq. (5.41). This formula is, however, also valid when the Coulomb interaction is large $U/t >> 1$, since in the derivation done in Sec. 5.2 the intercluster hopping was treated perturbatively with respect the Coulomb interaction. The unperturbed propagator of the auxiliary fermions was given by V and the lowest-order contribution ($R = 1$) to the self-energy was $\widehat{\Sigma} = \widehat{G}$, which leads to the same equation.

5.4 Semimetal-insulator transition for the honeycomb lattice

In this section, cluster perturbation theory is applied to the honeycomb lattice. The clusters are chosen as in Fig. 5.6. A single cluster is chosen as the unit cell of the honeycomb lattice and thus contains $L = 2$ lattice sites. A single cluster initially (for the exact diagonalization) contains two electrons with antiparralel spins ($N_\uparrow = N_\downarrow = 1$). The superlattice is a triangular lattice which has the same lattice vectors $\mathbf{R}_1$ and $\mathbf{R}_2$ as the honeycomb lattice

$$\mathbf{R}_1 = (\frac{\sqrt{3}}{2}, \frac{3}{2})a, \quad \mathbf{R}_2 = (-\frac{\sqrt{3}}{2}, \frac{3}{2})a. \tag{5.59}$$

The hopping matrix in the reciprocal space for this choice of clusters is given by

$$V(\mathbf{Q}) = -t \begin{pmatrix} 0 & e^{-i\mathbf{Q}\cdot\mathbf{R}_1} + e^{-i\mathbf{Q}\cdot\mathbf{R}_2} \\ e^{i\mathbf{Q}\cdot\mathbf{R}_1} + e^{i\mathbf{Q}\cdot\mathbf{R}_2} & 0 \end{pmatrix} \tag{5.60}$$

$$= -t \begin{pmatrix} 0 & e^{-i(\frac{\sqrt{3}}{2}Q_x + \frac{3}{2}Q_y)} + e^{i(\frac{\sqrt{3}}{2}Q_x - \frac{3}{2}Q_y)} \\ e^{i(\frac{\sqrt{3}}{2}Q_x + \frac{3}{2}Q_y)} + e^{i(-\frac{\sqrt{3}}{2}Q_x + \frac{3}{2}Q_y)} & 0 \end{pmatrix} \tag{5.61}$$

The Green's function $\mathcal{G}(\mathbf{Q}, \omega)$ can then be calculated using Eq. (5.44). It was rather difficult for the one dimensional chain to express this Green's function in

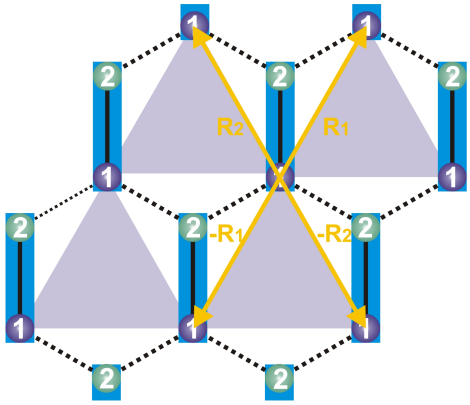

Figure 5.6: The honeycomb lattice with clusters containing $L = 2$ sites with superlattice vectors $\mathbf{R}_1$ and $\mathbf{R}_2$.

the reciprocal space of the original lattice. For the situation at hand, however, the reciprocal space for the superlattice is the same as the reciprocal space of the cluster, because the clusters are the unit cells of the honeycomb lattice. Therefore, $\mathcal{G}(\mathbf{Q}, \omega)$ can be directly used as the cluster perturbation Green's function $\mathcal{G}_{cpt}(\mathbf{Q}, \omega)$.

The density of states for different values of U/D, where $D = 3t$, is shown in Fig. 5.8. For $U = 0D$, the density of states obtained is the same as the non-interacting density of states calculated in Sec. 3.1 (See Fig. 4.5). When the Coulomb interaction is increased, the density of states near the Fermi energy does not change. This is very different from the single-site DMFT in Ch. 4.

To obtain a more precise value of the critical value of the Coulomb interaction strength, we examine the spectral weight. A colorplot of the spectral weight is shown in Fig. 5.9 as a function of the frequency ω and wavevector $\mathbf{k}$. The wavevector walks over the irreducible Brillouin zone of the honeycomb lattice shown in Fig. 5.7. At $U = 0$ there is a high value of the spectral weight at the point K of the reduced Brillouin zone corresponding to the Dirac point. When the Coulomb interaction increases the Dirac point seems to move towards the point M. It can be analytically shown that Dirac points do not move in an isotropic honeycomb lattice [36]. In the cluster perturbation theory the bonds within clusters are treated differently than the bonds between sites located in different clusters. This probably causes the Dirac point to move. Another possibility is that the interaction spontaneously breaks the isotropy. To confirm this however larger clusters should be considered. It can be clearly seen from Fig. 5.9 that the semimetal-insulator transition occurs at a value $U_c = 1.25D = 3.75t$.

The results obtained in this work at $T = 0$, using the cluster perturbation

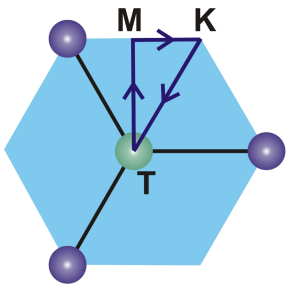

Figure 5.7: Brillouin zone of the Honeycomb lattice. The irriducable Brillouin zone is surrounded by the dark blue triangle.

theory, are close to the results of Ref [27,28]. Wu *et al.* [27] used continuous time Quantum Monte Carlo simulations to study the honeycomb lattice. Their results show that the density of states around the Dirac point does not depend on the interaction strength for $U < U_c$. The semimetal-insulator transition occurs at $U_c = 3.3t$. Meng *et al.* [28] did quantum Monte Carlo simulations and find a transition to a gapped spin-liquid state for $U_c = 3.5$.

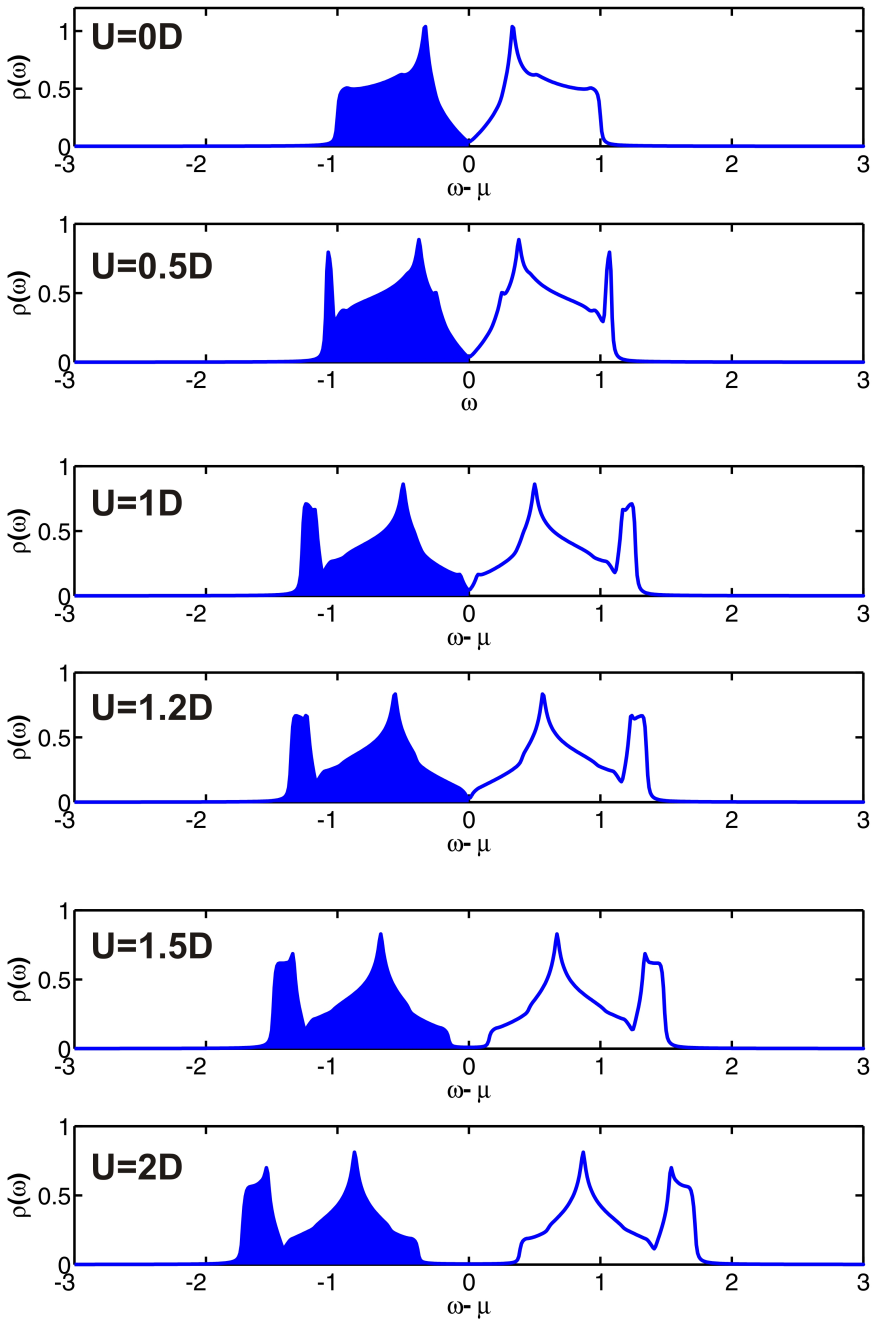

Figure 5.8: Density of states for the Honeycomb lattice obtained by CPT with $L = 2$ for $U/D = 0, 0.5, 1, 1.2, 1.5, 2$ at $T = 0$.

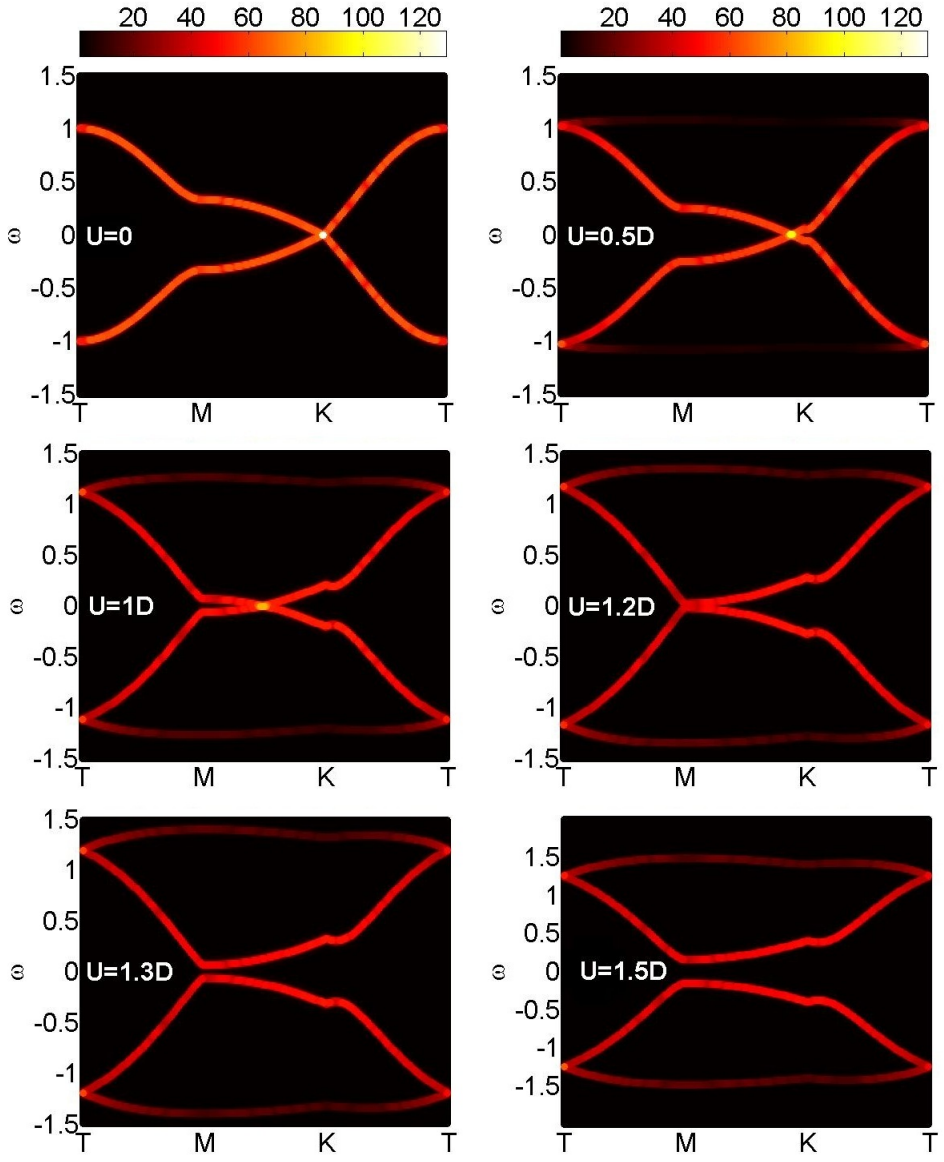

Figure 5.9: Spectral weight for the honeycomb lattice as a function of the frequency ω and the wavevector $\mathbf{k}$ for $U/D = 0, 0.5, 1, 1.2, 1.3, 1.5$. The wavevector walks over the first Brillioun zone depicted in Fig. 5.7

Chapter 6

Conclusion & Discussion

We studied the Hubbard model on a two-dimensional honeycomb lattice at half filling. A real material that has a two-dimensional honeycomb structure and one electron per site is graphene. We looked at the semimetal-insulator transition that is expected to occur when the ratio between the Coulomb interaction strength U and the on-site kinetic energy t of the electrons is increased, similar to the Mott transition observed in transition metal oxides. This transition has not jet been observed in graphene. We used two different numerical methods, single site Dynamical Mean Field Theory and Cluster Perturbation Theory, to obtain critical values for the ratio U_c/t for this transition to occur.

Single-site Dynamical Mean Field Theory gives an exact solution for the Hubbard model in the limit of infinite lattice coordination ($z \to \infty$). In this limit the self-energy, which accounts for the Coulomb interaction between electrons, becomes independent of the wavevector [10]. The problem can, therefore, be reduced to a single quantum impurity site embedded in an effective medium. Quantum fluctuations at the impurity site are taken into account because the site and the effective medium can exchange electrons.

We calculated the density of states for the honeycomb lattice at different values of U/t, from which a critical value for the semimetal-insulator transition of $U_c/t = 9.3$ is obtained. For non-interacting electrons the density of states vanishes at the Fermi energy (Dirac point). Our calculations show that upon increasing the Coulomb interaction strength, the system goes from a semimetal state to a metallic state and then to an insulating state which seems rather unphysical.

Single site DMFT neglects the wavevector dependence of the self-energy and, therefore, only includes local electron correlations. For a one-dimensional chain ($z = 2$), the limit of infinite lattice coordination is invalid and non-local electron correlations cannot be neglected [11]. To check whether non-local electron correlations are important for the honeycomb lattice (z=3) a second numerical

method was used called Cluster Perturbation Theory.

In this approach the lattice is divided into small identical clusters. The Hubbard Hamiltonian is solved exactly on the cluster using the Lanczos method [32] for exact diagonalization. The hopping of electrons between sites belonging to different clusters is treated by perturbation theory.

We showed that CPT can describe non-local correlations properly and gives the correct result for a one-dimensional chain. A critical value for the semimetal-insulator transition for the honeycomb lattice of $U_c = 3.75t$ (zero temperature) was obtained using a cluster containing two sites. Below the critical value U_c/t, the density of states near the Dirac point is independent of the Coulomb interaction strength. This result is very different from the results obtained by single-site DMFT where the non-local electron correlations where neglected. The value we obtained using CPT is close to the values obtained by Ref. [27] $U_c = 3.3t$ (CDMFT+QMC) and Ref. [28] $U_c = 3.5t$ (QMC) for a two-dimensional honeycomb lattice.

In graphene the ratio between the Coulomb interaction strength and the kinetic energy of the electrons $U/t \approx 2.2 - 4.4$. This ratio can be controlled by growing graphene on substrates with different dielectric constants. The value obtained by Cluster Perturbation Theory for the semimetal-insulator transition $U_c/t = 3.5$ is close to the ratio in graphene. Graphene, however, is conducting and a transition to an insulating state has not jet been observed. In graphene non-local Coulomb interactions are expected to be important [37] which are neglected in the Hubbard model. To improve our results the non-local Coulomb interactions should be taken into account and larger cluster sizes should be used.

Acknowledgment

In the last year many people contributed, directly or indirectly to the success of this project. I am grateful to all and I will mention a few in particular. First and foremost, Maxim Mostovoy whom I have been so fortunate and proud to have as a supervisor. I have always admired his teaching talents. He also gave me the opportunity to do part of my research at Osaka university, Japan.

My stay in japan turned out as an amazing academic and cultural experience, which I will never forget. I would like thank Prof. Ogawa, who immediately made me feel welcome in his group. He encouraged me to work hard and taught me a lot about Japan. I am very grateful to prof. Asano and prof. Ohashi, who guided me during my stay in Japan. We had many discussions on physics, and they taught me a lot of numerical techniques. My thesis would not have it's current form without them.

I also like to thank my other Group members at Osaka university and Groningen university.

Appendix A

Green's Functions

To describe many body systems it is sometimes more convenient to use Green's functions instead of the wavefunction formalism. In this appendix Green's functions will be discussed briefly. A more detailed description on Green's function can be found in Ref. [34,35]. We will start by defining the single-particle Green's function and calculate the representation in Fourier space in the case of non-interacting electrons. In Sec. A.2 we will treat the Coulomb interaction between electrons perturbatively for the Hubbard model in the limit of infinite dimensions. The method of the self-energy is explained and Dyson's equation will be derived. In Sec. 3.3 a practical calculation of the Green's function for non-interacting electrons for the Anderson model is given, which is used in chapter 3.

A.1 Free Fermion Green's function

In many body systems Green's functions are used as correlation functions. The one-particle Green's function using creation $\psi^\dagger_\sigma(\mathbf{r},t)$ and annihilation $\psi_\sigma(\mathbf{r},t)$ operators for a fermion to be created/annihilated at a position $\mathbf{r}$ at a time t can be defined as

$$\mathcal{G}_\sigma(\mathbf{r}_2,t_2,\mathbf{r}_1,t_1) = -i < \Phi_0 | T_t(\psi_\sigma(\mathbf{r}_2,t_2)\psi^\dagger_\sigma(\mathbf{r}_1,t_1))|\Phi_0 >, \tag{A.1}$$

where Φ_0 denotes the ground state of the system and T is the Dyson time ordered product defined as

$$T_t(\psi_\sigma(\mathbf{r}_2,t_2)\psi^\dagger_\sigma(\mathbf{r}_1,t_1)) = \begin{cases} \psi_\sigma(\mathbf{r}_2,t_2)\psi^\dagger_\sigma(\mathbf{r}_1,t_1) & \text{if } t_1 < t_2 \\ -\psi^\dagger_\sigma(\mathbf{r}_1,t_1)\psi_\sigma(\mathbf{r}_2,t_2) & \text{if } t_2 > t_1. \end{cases} \tag{A.2}$$

The minus sign in the time ordered product for $t_2 > t_1$ results from the interchange of two fermion operators. For $t_2 > t_1$, the Green's function describes the probability that an added electron to the system at position $\mathbf{r}_1$ and time t_1, has a position $\mathbf{r}_2$ after propagating for a time $t_2 - t_1$. For $t_2 < t_1$ the Green's

function describes the propagation of a hole. Note that the electron at the time t_1 is in the same state as at the time t_2. In many body systems it is often convenient to use the imaginary time Green's function, also called Matsubara Green's function

$$\mathcal{G}_\sigma(\mathbf{r}_2,\tau_2,\mathbf{r}_1,\tau_1) = - < \Phi_0|\Gamma_\tau(\psi_\sigma(\mathbf{r}_2,\tau_2)\psi^\dagger_\sigma(\mathbf{r}_1,\tau_1))|\Phi_0 >, \tag{A.3}$$

where $\tau = it$ is the imaginary time. In order to lighten notation $\mathbf{r}_1$ can be chosen as the origin and τ_1 can be taken equal to zero, so that

$$\mathcal{G}_\sigma(\mathbf{r}_2,\tau_2,0,0) = \mathcal{G}(\mathbf{r},\tau) \tag{A.4}$$

The Fourier transform for the creation and annihilation operator to momentum space is given by

$$c_{\mathbf{k}\sigma}(\tau) = \frac{1}{\sqrt{V}}\int d^3x e^{-i\mathbf{k}\cdot\mathbf{r}}\psi_\sigma(\mathbf{r},\tau) \tag{A.5}$$

$$c^\dagger_{\mathbf{k}\sigma}(\tau) = \frac{1}{\sqrt{V}}\int d^3x e^{i\mathbf{k}\cdot\mathbf{r}}\psi^\dagger_\sigma(\mathbf{r},\tau) \tag{A.6}$$

The inverse Fourier transform to coordination space is

$$\psi_\sigma(\mathbf{r},\tau) = \frac{1}{\sqrt{V}}\sum_k e^{i\mathbf{k}\cdot\mathbf{r}}c_{\mathbf{k}\sigma}(\tau) \tag{A.7}$$

$$\psi^\dagger_\sigma(\mathbf{r},\tau) = \frac{1}{\sqrt{V}}\sum_k e^{-i\mathbf{k}\cdot\mathbf{r}}c^\dagger_{\mathbf{k}\sigma}(\tau). \tag{A.8}$$

Performing the Fourier transform, the one particle Green's function in Eq. A.4 can be rewritten as

$$\mathcal{G}_\sigma(\mathbf{k},\tau) = - < \Phi_0|\Gamma_\tau(c_{\mathbf{k}\sigma}(\tau)c^\dagger_{\mathbf{k}\sigma}(0))|\Phi_0 > . \tag{A.9}$$

The time dependence of the operators is from quantum mechanics

$$c_{\mathbf{k}\sigma}(\tau) = e^{\mathcal{H}\tau}c_{\mathbf{k}\sigma}e^{-\mathcal{H}\tau}. \tag{A.10}$$

The derivative with respect to the imaginary time is then

$$\frac{dc_{\mathbf{k}\sigma}}{d\tau} = e^{\mathcal{H}\tau}[\mathcal{H},c_{\mathbf{k}\sigma}]e^{-\mathcal{H}\tau} \tag{A.11}$$

Using the Hamiltonian for free fermions in momentum space

$$\mathcal{H} = \sum_{\mathbf{k}\sigma}(\epsilon_k - \mu)c^\dagger_{\mathbf{k}\sigma}c_{\mathbf{k}\sigma}, \tag{A.12}$$

this expression can be written as

$$\frac{dc_{\mathbf{k}\sigma}}{d\tau} = -(\epsilon_k - \mu)c_{\mathbf{k}\sigma}. \tag{A.13}$$

From this the time-dependence of the of the creation and annihilation operators follows

$$c_{\mathbf{k}\sigma}(\tau) = e^{-(\epsilon_k-\mu)\tau}c_{\mathbf{k}\sigma} \quad (A.14)$$

$$c^\dagger_{\mathbf{k}\sigma}(\tau) = e^{-(\epsilon_k-\mu)\tau}c^\dagger_{\mathbf{k}\sigma}. \quad (A.15)$$

Taking the derivative with respect to imaginary time of the one-particle Green's function, results in

$$\frac{d}{d\tau}\mathcal{G}(\mathbf{k},\tau) = -(\epsilon_k-\mu)\mathcal{G}(\mathbf{k},\tau) - \delta(\tau) < \Phi_0|\{c_{\mathbf{k}\sigma}, c^\dagger_{\mathbf{k}\sigma}\}|\Phi_0 > \quad (A.16)$$

The Fourier transform of the Green's function with respect to imaginary time is defined as

$$\mathcal{G}_\sigma(\mathbf{k},\omega_m) = \int_0^\beta d\tau e^{i\omega_m\tau}\mathcal{G}_\sigma(\mathbf{k},\tau) \quad (A.17)$$

$$\mathcal{G}_\sigma(\mathbf{k},\tau) = T\sum_{\omega_m} e^{-i\omega_m\tau}\mathcal{G}_\sigma(\mathbf{k},\omega_m). \quad (A.18)$$

Where ω_m is the Matsubara frequency. The Matsubara Green's function is an anti-periodic function with period $\beta = 1/T$ (inverse temperature)

$$\mathcal{G}_\sigma(\mathbf{k},\tau) = -\mathcal{G}_\sigma(\mathbf{k},\tau+\beta). \quad (A.19)$$

From this it follows that the Matsubara frequencies ω_m in Eq. A.18 are odd

$$\omega_m = (2m+1)\pi T \quad (A.20)$$

Taking the Fourier transform gives the solution to the differential equation (Eq. (A.16)) of the free fermion Green's function

$$\mathcal{G}_\sigma(\mathbf{k},\omega_m) = \frac{1}{i\omega_m + \mu - \epsilon_{\mathbf{k}}}. \quad (A.21)$$

The poles of the Green's function occur at the energies of the particles. The Matsubara Green's function is related in the following way to two other Green's functions that are particularly useful and important

$$\mathcal{G}_\sigma(\mathbf{k},\omega_m) = \begin{cases} G^R_\sigma(\mathbf{k},i\omega_m) & \text{for } \omega_m > 0 \\ G^A_\sigma(\mathbf{k},i\omega_m) & \text{for } \omega_m < 0. \end{cases} \quad (A.22)$$

Here G^R_σ is the retarded Green's function which is by definition

$$\mathcal{G}^R_\sigma(\mathbf{r}_2,t_2,\mathbf{r}_1,t_1) = -i\theta(t_2-t_1) < \Phi_0|\{\psi_\sigma(\mathbf{r}_2,t_2), \psi^\dagger_\sigma(\mathbf{r}_1,t_1)\}|\Phi_0 >, \quad (A.23)$$

and G^A_σ is the advanced Green's function

$$\mathcal{G}^A_\sigma(\mathbf{r}_2,t_2,\mathbf{r}_1,t_1) = i\theta(t_1-t_2) < \Phi_0|\{\psi_\sigma(\mathbf{r}_2,t_2), \psi^\dagger_\sigma(\mathbf{r}_1,t_1)\}|\Phi_0 > . \quad (A.24)$$

A.2 Self-energy

The Hubbard model describes the propagation of interacting electrons through a material. The Hamiltonian in momentum space is given by Eq. 2.20

$$\mathcal{H} = \sum_{\mathbf{k}\sigma}(\epsilon_{\mathbf{k}} - \mu)c^{\dagger}_{\mathbf{k}\sigma}c_{\mathbf{k}\sigma} + \frac{U}{L}\sum_{\mathbf{k}\mathbf{k}'\mathbf{q}\neq 0,\sigma} c^{\dagger}_{\mathbf{k}-\mathbf{q}\sigma}c^{\dagger}_{\mathbf{k}'+\mathbf{q},-\sigma}c_{\mathbf{k}',-\sigma}c_{\mathbf{k}\sigma}, \tag{A.25}$$

where the first term corresponds to the Hamiltonian for free fermions in Eq. A.12. The Green's function describes the propagation from a point r' to a point r of an electron (hole) added to the system. In the Hubbard model the added electron (hole), can interact infinitely many times with the other electrons (holes) in the system during it's propagation. The scattering between two electrons, is shown in Fig. A.1.

In this section we will treat the Coulomb interaction between electrons perturbatively and see how it contributes to the electron Green's function. The

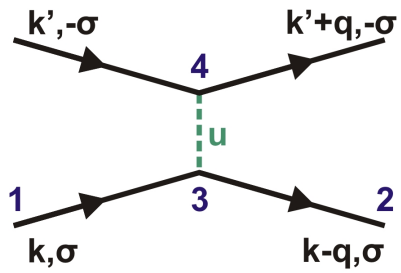

Figure A.1: An electron with initial momentum $\mathbf{k}$ added to the system at $1 = (\mathbf{r}, \tau)$, scatters with an electron of the system at the point 3 and propagates to 4.

Green's function in Eq. A.3 can be written as a functional integral over the Grassmann variables $\gamma^{\dagger}(\mathbf{r}, t)$ and $\gamma(\mathbf{r}, t)$ corresponding to the electron creation and annihilation operators respectively

$$\mathcal{G}_{\sigma}(\mathbf{r}_2, \tau_2, \mathbf{r}_1, \tau_1) = -\frac{\int D\gamma^{\dagger}D\gamma e^{-S_e(\gamma^{\dagger},\gamma)}\gamma_{\sigma}(\mathbf{r}_2, t_2)\gamma^{\dagger}_{\sigma}(\mathbf{r}_1, t_1)}{\int D\gamma^{\dagger}D\gamma e^{S_e(\gamma^{\dagger},\gamma)}}, \tag{A.26}$$

where S_e is the effective action. For the Hubbard model in infinite dimensions the effective action reduces to a single impurity site in an effective medium and is given by (Eq. (3.24))

$$\begin{aligned} S_e &= -\int_0^{\beta} d\tau \int_0^{\beta} d\tau' \sum_{\sigma} \gamma^{\dagger}_{\sigma}(\tau)[\mathcal{G}^0_{\sigma}(\tau - \tau')]^{-1}\gamma_{\sigma}(\tau') \\ &\quad + U\int_0^{\beta} d\tau n_{\uparrow}(\tau)n_{\downarrow}(\tau). \end{aligned} \tag{A.27}$$

The effective action for non-interacting electrons is defined as S_0 and is quadratic in the Grassmann fields. The Coulomb interaction part is treated perturbatively and can be expanded to first order in U which leads to

$$\mathcal{G}_\sigma(\tau_2,\tau_1) = -\frac{\int D\gamma^\dagger D\gamma e^{-S_0(\gamma^\dagger,\gamma)}[1-U\int_0^\beta d\tau n_\uparrow(\tau)n_\downarrow(\tau)]\gamma_\sigma(\tau_2)\gamma_\sigma^\dagger(\tau_1)}{\int D\gamma^\dagger D\gamma e^{-S_0(\gamma^\dagger,\gamma)}[1-U\int_0^\beta d\tau n_\uparrow(\tau)n_\downarrow(\tau)]} \tag{A.28}$$

Dividing both the numerator and denominator by $\int D\gamma^\dagger D\gamma e^{-S_0}$ gives

$$\begin{aligned}
\mathcal{G}_\sigma(\tau_2,\tau_1) &= -\frac{<\gamma_\sigma(\tau_2)\gamma_\sigma^\dagger(\tau_1)>_0 -U\int_0^\beta d\tau <n_\uparrow(\tau)n_\downarrow(\tau)\gamma_\sigma(\tau_2)\gamma_\sigma^\dagger(\tau_1)>_0}{1-U\int_0^\beta d\tau <n_\uparrow(\tau)n_\downarrow(\tau)>_0} \\
&\approx -<\gamma_\sigma(\tau_2)\gamma_\sigma^\dagger(\tau_1)>_0 +U\int_0^\beta d\tau <\gamma_\sigma(\tau_2)\gamma_\sigma^\dagger(\tau_1)>_0<n_\uparrow(\tau)n_\downarrow(\tau)>_0 \\
&\quad -U\int_0^\beta d\tau <n_\uparrow(\tau)n_\downarrow(\tau)\gamma_\sigma(\tau_2)\gamma_\sigma^\dagger(\tau_1)>_0,
\end{aligned} \tag{A.29}$$

where $<..>_0$ denotes the average over the unperturbed (U=0) action. The Wick theorem states that the average of a product of creation and annihilation operators can be written as the product of all possible pairwise averages.

$$<ABCD>=<AB><CD>-<AC><BD>+<AD><BC> \tag{A.30}$$

The Wick theorem applies to Gaussian distribution functions and, therefore, the non-perturbed effective action has to be quadratic in creation/annihilation operators. Using the Wick theorem, the last average for the Green's function $\mathcal{G}_\uparrow(\tau_2,\tau_1)$ in Eq. A.29 can be rewritten

$$\begin{aligned}
<n_\uparrow(\tau)n_\downarrow(\tau)\gamma_\sigma(\tau_2)\gamma_\sigma^\dagger(\tau_1)>_0 &= <\gamma_\uparrow(\tau)\gamma_\uparrow^\dagger(\tau)\gamma_\downarrow(\tau)\gamma_\downarrow^\dagger(\tau)\gamma_\uparrow(\tau_2)\gamma_\uparrow^\dagger(\tau_1)>_0 \\
&= <n_\uparrow(\tau)n_\downarrow(\tau)>_0<\gamma_\uparrow(\tau_2)\gamma_\uparrow^\dagger(\tau_1)>_0 \\
&\quad +<\gamma_\downarrow(\tau)\gamma_\downarrow^\dagger(\tau)>_0<\gamma_\uparrow(\tau)\gamma_\uparrow^\dagger(\tau_1)>_0<\gamma_\uparrow(\tau_2)\gamma_\uparrow^\dagger(\tau)>_0
\end{aligned} \tag{A.31}$$

Note that all other pairwise averages are equal to zero. Filling this expression into Eq. (A.29) leads to

$$\begin{aligned}
\mathcal{G}_\uparrow(\tau_2,\tau_1) &= -<\gamma_\sigma(\tau_2)\gamma_\sigma^\dagger(\tau_1)>_0 \\
&\quad +U\int_0^\beta d\tau <\gamma_\downarrow(\tau)\gamma_\downarrow^\dagger(\tau)>_0<\gamma_\uparrow(\tau)\gamma_\uparrow^\dagger(\tau_1)>_0<\gamma_\uparrow(\tau_2)\gamma_\uparrow^\dagger(\tau)>_0 \\
&= \mathcal{G}_\uparrow^0(\tau_2,\tau_1) - U\int_0^\beta d\tau \mathcal{G}_\downarrow^0(\tau,\tau)\mathcal{G}_\uparrow^0(\tau,\tau_1)\mathcal{G}_\sigma^0(\tau_2,\tau)
\end{aligned} \tag{A.32}$$

The Green's function for interacting electrons can thus be written in terms of the bare Green's functions. The different terms in Eq. (A.32) can be represented

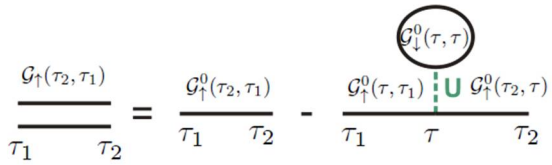

Figure A.2: Feynman diagrams up to first order in the Coulomb interaction U.

by Feynman diagrams (Fig. A.2). A Green's function for interacting electrons is represented by a double solid line and the bare Green's function by a single solid line. At an interaction point four lines come together and a dashed green line is used. The diagram with the interaction vertex, actually describes the interaction of a single electron, with the average density of all other electrons which corresponds to the Hartree approximation [34]. If the exponent in Eq. (A.28) was expanded to second order in U, extra diagrams contribute to the Green's function for interacting electrons. Two of them are shown in Fig. A.3. Clearly the first second order diagram in the figure is a repetition of the first

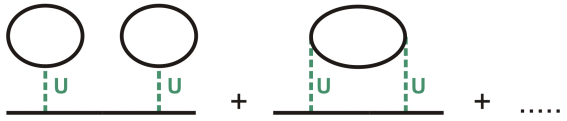

Figure A.3: Two Feynman diagrams which are of second order in the Coulomb interaction U.

order diagram shown in Fig. A.2. There is a technique which allows one to take into account all repetition diagrams to infinite order in U. First one has to select the irreducible diagrams, which are diagrams that cannot be divided into two parts by cutting a single continuous line. Here we will consider the irreducible diagrams to second order in U. The sum of these irreducible diagrams is denoted by the self-energy Σ. Higher order diagrams containing the same interaction

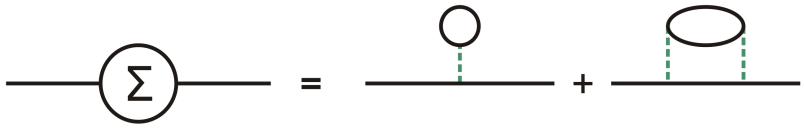

Figure A.4: The self-energy containing two irreducible diagrams.

multiple times, can then be written as a repetition of the self-energy. This is shown in Fig. A.5 or

$$\mathcal{G} = \mathcal{G}^0 + \mathcal{G}^0\Sigma\mathcal{G}^0 + \mathcal{G}^0\Sigma\mathcal{G}^0\Sigma\mathcal{G}^0 + \mathcal{G}^0\Sigma\mathcal{G}^0\Sigma\mathcal{G}^0\Sigma\mathcal{G}^0 + ... \tag{A.33}$$

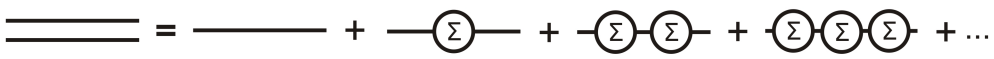

Figure A.5: Higher order diagrams are taken into account by repetition of the self-energy which contains irreducible diagrams.

This series can be rewritten into the Dyson equation

$$\begin{aligned} \mathcal{G} &= \mathcal{G}^0(1 + \Sigma\mathcal{G}^0 + (\Sigma\mathcal{G}^0)^2 + (\Sigma\mathcal{G}^0)^3 + ...) \\ &= \mathcal{G}^0(1 - \Sigma\mathcal{G}^0)^{-1} \\ &= \frac{1}{(\mathcal{G}^0)^{-1} - \Sigma}. \end{aligned} \tag{A.34}$$

For the infinite dimensional Hubbard model the self-energy is independent of the coordinates $\mathbf{r}$ since a single site is considered. In general, diagrams connecting the site i and the site j also contribute to the self-energy. Taken the Fourier transform to momentum space and with respect to time the Dyson equation can be written as

$$\begin{aligned} \mathcal{G}(\omega_m, \mathbf{k}) &= \frac{1}{(\mathcal{G}^0(\omega_m, \mathbf{k}))^{-1} - \Sigma(\omega_m, \mathbf{k})} \\ &= \frac{1}{i\omega_m + \mu - \epsilon_{\mathbf{k}} - \Sigma(\omega_m, \mathbf{k})}. \end{aligned} \tag{A.35}$$

A.3 Bare Green's function in Anderson impurity model

In this section the Bare Green's function for the Anderson model will be calculated. The Hamiltonian for the Anderson model is

$$\mathcal{H}_A = \sum_{\mathbf{k}\sigma} \epsilon_{\mathbf{k}} c^\dagger_{\mathbf{k}\sigma} c_{\mathbf{k}\sigma} + \sum_\sigma \epsilon_d d^\dagger_\sigma d_\sigma + U d^\dagger_\uparrow d_\uparrow d^\dagger_\downarrow d_\downarrow + \sum_{\mathbf{k}\sigma} [V_{kd} c^\dagger_{\mathbf{k}\sigma} d_\sigma + h.c.]. \tag{A.36}$$

The bare Green's function is the single-particle Green's function in the case of non-interacting electrons $U = 0$

$$\mathcal{G}_{dd}(\tau) = - < \Phi_0 | \Gamma_\tau (d_\sigma(\tau) d^\dagger_\sigma(0)) | \Phi_0 > . \tag{A.37}$$

Taking the derivative with respect to imaginary time and using that the derivative of the theta function is the delta function gives the following

$$\frac{\partial}{\partial\tau}\mathcal{G}_{dd}(\tau) = -\delta(\tau) - < \Gamma_\tau \frac{\partial d_\sigma(\tau)}{\partial\tau} d^\dagger_\sigma(0) > . \tag{A.38}$$

The time dependence of the operators is given in Eq. (A.13). The commutator in Eq. (A.13) for the Anderson model with U=0 is

$$[\mathcal{H}_{A0}, d_\sigma] = -\epsilon_d d_\sigma - \sum_{\mathbf{k}} V_k c_{k\sigma}. \tag{A.39}$$

Substituting this expression in Eq. (A.38) gives

$$\frac{\partial}{\partial\tau}\mathcal{G}_{dd}(\tau) = -\delta(\tau) - \epsilon_d\mathcal{G}_{dd}(\tau) - \sum_{\mathbf{k}} V_{\mathbf{k}}\mathcal{G}_{\mathbf{k}d}(\tau), \tag{A.40}$$

where

$$\mathcal{G}_{\mathbf{k}d} = - < \Phi_0|\Gamma_\tau(c_{\mathbf{k}\sigma}(\tau)d^\dagger_\sigma(0))|\Phi_0 > . \tag{A.41}$$

Now taking the Fourier transform with respect to time on both sites leads to the following equation

$$(i\omega_m - \epsilon_d)\mathcal{G}_{dd}(i\omega_m) = 1 + \sum_{\mathbf{k}} V_{\mathbf{k}}\mathcal{G}_{kd}(i\omega_m) \tag{A.42}$$

A similar calculation can be done for $\mathcal{G}_{\mathbf{k}d}$ which gives

$$\frac{d}{d\tau}\mathcal{G}_{\mathbf{k}d}(\tau) = -\epsilon_{\mathbf{k}}\mathcal{G}_{\mathbf{k}d}(\tau) - V^*_{\mathbf{k}}\mathcal{G}_{dd}(\tau). \tag{A.43}$$

Taking the Fourier transform leads to the following

$$\mathcal{G}_{\mathbf{k}d}(i\omega_m) = \frac{V^*_{\mathbf{k}}}{i\omega_m - \epsilon_d}\mathcal{G}_{dd}(i\omega_m). \tag{A.44}$$

Substituting this in Eq. (A.42), results in an expression for the bare Green's function for the Anderson model

$$\begin{aligned}
[\mathcal{G}_{dd}(i\omega_m)]^{-1} &= i\omega_m - \epsilon_d - \sum_{\mathbf{k}} \frac{|V_{\mathbf{k}}|^2}{i\omega_m - \epsilon_{\mathbf{k}}} \\
&= i\omega_m - \epsilon_d - \int_{-\infty}^{\infty} d\epsilon \frac{\sum_{\mathbf{k}} |V_{\mathbf{k}}|^2 \delta(\epsilon - \epsilon_{\mathbf{k}})}{i\omega_m - \epsilon}
\end{aligned} \tag{A.45}$$

Appendix B

Integral semi circular density of states

The integral that has to be solved for the lattice Green function for the Bethe lattice in infinite dimensions is

$$\mathcal{G}_{lat}(i\omega_m) = \frac{2}{\pi D^2}\int_{-D}^{D} d\epsilon \frac{\sqrt{D^2-\epsilon^2}}{i\omega_m + \mu - \epsilon - \Sigma(i\omega_m)}. \tag{B.1}$$

Here $D = 2t$ and is the radius of the semicircle (DOS). The integral can be solved using Cauchy's Residue theorem. Performing the substitution $\epsilon = 2t\cos(\theta)$ the integral can be rewritten as

$$\mathcal{G}_{lat}(i\omega_m) = \frac{1}{\pi}\int_{-\pi}^{\pi} d\theta \frac{\sin^2(\theta)}{i\omega_m + \mu - \Sigma(i\omega_m) - 2t\cos(\theta)}. \tag{B.2}$$

This integral can be rewritten as a contour integral over the unit circle (c_1) in the complex plane. Making the substitution $z = e^{i\theta}$ gives

$$\mathcal{G}_{lat}(i\omega_m) = \oint_{c_1} \frac{dz}{4\pi i z} \frac{(z-\frac{1}{z})^2}{i\omega_m + \mu - \Sigma(i\omega_m) - t(z+\frac{1}{z})}. \tag{B.3}$$

Multiplying numerator and denominator by z^2 and rearranging terms leads to

$$\mathcal{G}_{lat}(i\omega_m) = \frac{1}{4\pi i t}\oint_{c_1} dz \frac{(z^2-1)^2}{z^2(z-\alpha_+)(z-\alpha_-)}, \tag{B.4}$$

where

$$\alpha_\pm = \frac{1}{2t}(i\omega_m + \mu - \Sigma(i\omega_m) \pm \sqrt{((i\omega_m + \mu - \Sigma(i\omega_m))^2 - 4t^2)}). \tag{B.5}$$

So the function has a second order pole at $z = 0$ and two simple poles at $z = \alpha_+$ and $z = \alpha_-$. The residues of the poles are

$$z = 0, \quad Res = \frac{\alpha_- + \alpha_+}{4\pi i t} \tag{B.6}$$

$$z = \alpha_\pm, \quad Res = \frac{\alpha_\pm - \alpha_\mp}{4\pi i t}. \tag{B.7}$$

Note that $\alpha_+\alpha_- = 1$. For convenience, $\nu(i\omega_m)$ is defined as

$$\nu(i\omega_m) = i\omega_m + \mu - \Sigma(i\omega_m). \tag{B.8}$$

The poles that lie within the unit circle only contribute to the integral. The second order pole at $z = 0$, therefore, always contributes. It depends on the value of $\nu(i\omega_m)$ whether α_+ and α_- contribute. All cases are treated below. If both α_+ and α_- are in the unit circle their contributions to the integral cancel.

If $\mathrm{Im}[\nu(i\omega_m)]= 0$ then three different cases arise.
1) $\nu(i\omega_m)^2 > 4t^2$.
Then α_+ is in the unit circle when $\nu(i\omega_m) < 0$.
Then α_- is in the unit circle when $\nu(i\omega_m) > 0$.
2) $\nu(i\omega_m)^2 < 4t^2$
Then α_+ and α_- are in the unit circle at the same time (no contribution).
3) $\nu(i\omega_m)^2 = 4t^2$
Then $\alpha_+ = \alpha_-$ and a second order pole is formed. It's residue is however equal to zero.

If $\mathrm{Im}[\nu(i\omega_m)]\neq 0$
Then two cases arise
1) $\mathrm{Im}[\nu(i\omega_m)]> 0$
Then only α_- lies within the unit circle and contributes.
2) $\mathrm{Im}[\nu(i\omega_m)]< 0$
Then only α_+ lies within the unit circle and contributes.

The integral can now be calculated for each case separately by taking the sum of all residues and multiplying by $2\pi i$. The result is summarized below

$$\mathcal{G}_{lat} = \left\{ \begin{array}{ll} \frac{2}{\nu(i\omega_m)+\eta(i\omega_m)\sqrt{\nu(i\omega_m)^2-4t^2}} & (\eta(i\omega_m) = \pm 1) \\ \frac{\nu(i\omega_m)}{2t^2} & (\eta(i\omega_m) = 0) \end{array} \right\} \tag{B.9}$$

$$\eta(i\omega_m) = \left\{ \begin{array}{ll} 0 & \mathrm{Im}(\nu(i\omega_m))= 0 \text{ and } |\mathrm{Re}(\nu(i\omega_m))| \leq 2t \\ +1 & \mathrm{Im}(\nu(i\omega_m))> 0 \text{ or } \mathrm{Im}(\nu(i\omega_m))= 0 \text{ and } \mathrm{Re}(\nu(i\omega_m))< -2t \\ -1 & \mathrm{Im}(\nu(i\omega_m))> 0 \text{ or } \mathrm{Im}(\nu(i\omega_m))= 0 \text{ and } \mathrm{Re}(\nu(i\omega_m))> 2t \end{array} \right.$$

Bibliography

[1] Fabian H.L. Essler et all, *The one dimensional Hubbard Model*. Cambridge University Press, 1st Edition, 2005.

[2] L. D. Landau and E. M. Lifshitz, *Quantum Mechanics*. Pergamon Press Oxford, 3rd impression, 1962.

[3] P. W. Anderson, *Concepts in Solids, lectures on the theory of solids*. World Scientific Publishing, 2003.

[4] Philip Phillips, *Advanced solid state physics*. Westview press, 2003.

[5] E. Fradkin, *Field theories of condensed matter systems*. Perseus Books Cambridge, 1991.

[6] C. Kittel, *Introduction to Solid State Physics, 8th Edition* John Wiley & Sons, 2005.

[7] M. Mostovoy *Introduction to condensed matter theory* (2010)

[8] A. Georges, G. Kothliar, W. Krauth and M.J. Rozenberg, Rev. Mod. Phys. **68**, 13 (1996).

[9] A. Georges and W. Krauth, Phys. Rev. B. **48**, 10 (1993).

[10] D. Vollhardt, *Dynamical Mean-Field Theory of Electronic Correlations in Models and Materials*. arXiv:1004.5069v2 (2010).

[11] C. J. Bolech, S. S. Kancharla, and G. Kotliar, Phys. Rev. B 67,075110 (2003).

[12] Z.Y. Meng, T. C. Lang, S. Wessel, F. F. Assaad and A. Muramatsu, Nature **464**, 847 (2010).

[13] S. Raghu, X.L. Qi, C. Honerkamp and S. C. Zhang Phys Rev. Lett. **100**, 156401 (2008).

[14] J. Nagamatsu, Norimasa Nakagawa, Takahiro Muranaka1 Yuji Zenitani1 and Jun Akimitsu, Nature **410**,63 (2001)

[15] V. N. Kotov, B. Uchoa, V. M. Pereira, A. H. Castro Neto and F. Guinea, arXiv:1012.3484v1.

[16] S. A. Jafari Eur. Phys. J. B 68, 537542 (2009).

[17] J. P. Hobson, W. A. Nierenberg, Phys. Rev. **89**, 662 (1953).

[18] H. P. Dahal, J. P. Julien, A.V. Balatsky, arxiv:0712.2836.

[19] J. M. Luttinger and J. C. Ward, Phys. Rev. **118**, 5 (1960).

[20] D. Sénéchal, D. Perez and M. Pioro-Ladriére, Phys. Rev. Lett. 522,84 (2000).

[21] D. Sénéchal, D. Perez and D. Plouffe, Phys. Rev. B 66, 075129 (2002).

[22] S. Pairault, D. Sénéchal and A.-M.S. Tremblay, Phys. Rev. Lett. **80**,5389 (1998)

[23] S. Pairault, D. Sénéchal and A.-M.S. Tremblay, Eur. Phys. J. B **16**,85 (2000)

[24] D. Sénéchal and A.-M.S. Tremblay, Phys. Rev. Lett **92**,16 (2004)

[25] E.R. Gagliano and C.A. Balserio, Phys. Rev. Lett. **59**, Number (26) (1987)

[26] W. Metzner, Phys. Rev. B **43**,8549 (1991).

[27] Wei Wu, Yao-Hua Chen, Hong-Shuai Tao, Ning-Hua Tong and Wu-Ming Liu Phys. Rev. B **82**, 245102 (2010).

[28] Z. Y. Meng, T. C. Lang, S. Wessel, F. F. Assaad, and A. Muramatsu, Nature **464**, 847 (2010).

[29] H.Q. Lin and J.E. Gubernatis, Exact diagonalization methods for quantum systems, Computers in Physics, Vol 7, No. 4 Jul/Aug (1993).

[30] P.W. Leung, Z. Liu, E. Manousakis, M. A. Novotny and P. E. Oppenheimer Phys. Rev. B **46**, 11 779 (1992).

[31] Y. Ohta, K. Tsutsui, W. Koshibae, T. Shimozato and S. Maekawa, Phys. Rev. B **46**, 14022 (1992).

[32] L. Komszik, *The Lanczos Method evolution and application*, Siam, (2003)

[33] G. Baym and C. Pethick, *Landau Fermi-Liquid Theory, concepts and applications*, John Wiley & Sons, inc. (1991)

[34] D. I. Khomshkii, *Basic aspects of the quantum theory of solids*, Cambridge university press (2010).

[35] G. Rickayzen, *Green's functions and condensed matter*, Acadamic press, (1980).

[36] K. Asano and C. Hotta, *preprint* arxiv:1104.2526 (2011).

[37] T. O. Wehling, E. Sasiogu, C. Friedrich, A. I. Lichtenstein, M. I. Katsnelson, and S. Blugel, *Strength of effective Coulomb interactions in graphene and graphite*, arXiv: 1101.4007 (2011).

[38] J. Hubbard, Proc Roy Soc A 276,N1363, 238 (1963).